Journal of Medicinal Chemistry

pubs.acs.org/jmc

Article

Discovery of a Selective and Orally Bioavailable FGFR2 Degrader for Treating Gastric Cancer

Lin Ma,[⊥] Yingying Li,[⊥] Ruixiang Luo,[⊥] Yuhan Wang, Jiaqi Cao, Weitao Fu, Bolan Qian, Lei Zheng, Longguang Tang, Xinting Lv, Lulu Zheng,* Guang Liang,* and Lingfeng Chen*

Cite This: https://doi.org/10.1021/acs.jmedchem.3c00150

Read Online

ACCESS | Metrics & More | Article Recommendations | Supporting Information

ABSTRACT: Abnormal activation of fibroblast growth factor receptors (FGFRs) results in the development and progression of human cancers. FGFR2 is frequently amplified or mutated in cancers; therefore, it is an attractive target for tumor therapy. Despite the development of several pan-FGFR inhibitors, their long-term therapeutic efficacy is hindered by acquired mutations and low isoform selectivity. Herein, we report the discovery of an efficient and selective FGFR2 proteolysis-targeting chimeric molecule, LC-MB12, that incorporates an essential rigid linker. LC-MB12 preferentially internalizes and degrades membrane-bound FGFR2 among the four FGFR isoforms; this may promote greater clinical benefits. LC-MB12 exhibits superior potency in FGFR signaling suppression and antiproliferative activity compared to the parental inhibitor. Furthermore, LC-MB12 is orally bioavailable and shows significant antitumor effects in FGFR2-dependent gastric cancer in vivo. Taken together, LC-MB12 is a candidate FGFR2 degrader for alternative FGFR2-targeting strategies and offers a promising starting point for drug development.

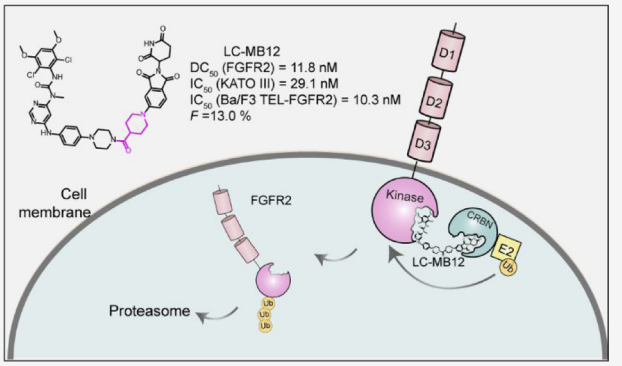

1. INTRODUCTION

The fibroblast growth factor (FGF) family involves four known receptors (FGFR1-4) that recognize 18 paracrine and endocrine fibroblast growth factor ligands (FGFs). This family of receptor tyrosine kinases (RTKs) is involved in regulating various physiological processes, including cell proliferation, differentiation, embryogenesis, and metabolic homeostasis.[1,2] Ligand-induced receptor dimerization results in precisely ordered tyrosine transphosphorylation of the intracellular kinase domain.[3] Following phosphorylation, two substrates (FRS2α and PLCγ) activate multiple cascade pathways, including PI3K-, MAPK-, and STAT-dependent signaling.[4] Dysregulation of FGF/FGFRs leads to oncogenesis and tumor progression. The oncogenic FGFR signaling pathway is primarily triggered by FGFR genetic alterations, including amplification, point mutations, and gene fusions.[2,5,6] For instance, FGFR2 amplification is frequently detected in 7.7% of patients with advanced gastric cancer through ctDNA sequencing.[7] Besides, multiple FGFR2 fusion proteins (such as FGFR2−PPHLN1 and FGFR2−CCDC6) are found in gastric cancer and cholangiocarcinoma that significantly promote cancer cell proliferation and tumorigenesis.[6,8] Thus, FGFR2 is an important target for tumor therapy.

Three generations of FGFR inhibitors have been developed because of the oncogenic role of FGFR signaling. First-generation FGFR inhibitors (such as derazantinib and ponatinib) are active against multiple RTKs, including PDGFRs, VEGFRs, and KIT.[9] To lower the risk of off-target related side effects, second-generation FGFR inhibitors, such as infigratinib (BGJ398), AZD4547, erdafitinib, and pemigatinib, have been developed with improved selectivity.[10] Infigratinib is a diaminopyrimidine derivative that selectively targets FGFR1-3. Currently, infigratinib is in a phase III study (NCT03773302) as a first-line treatment for cholangiocarcinoma patients harboring FGFR2 alterations and in a phase I study (NCT04424966) in patients with high-grade glioma carrying FGFR3−TACC3 fusions.[11] Futibatinib (TAS120) is a third-generation FGFR inhibitor that irreversibly targets the conserved cysteine residue of FGFR paralogs (Cys486 in FGFR1), thereby achieving an extended pharmacodynamic duration.[12]

Despite great progress in the development of FGFR-targeting drugs, the long-term efficacy of these inhibitors in cancer management is hampered by acquired resistance.[13] For example, infigratinib treatment leads to clinically observed

Received: January 26, 2023

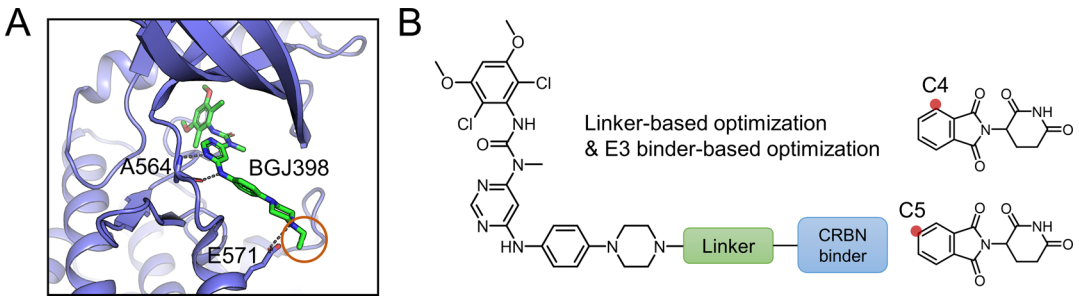

Figure 1. Rationale of the FGFR degrader design. (A) Structure of the BGJ398-FGFR1 complex. (B) Our PROTAC design strategy.

Scheme 1. Synthesis Route of Compound LC-MB1~15[a]

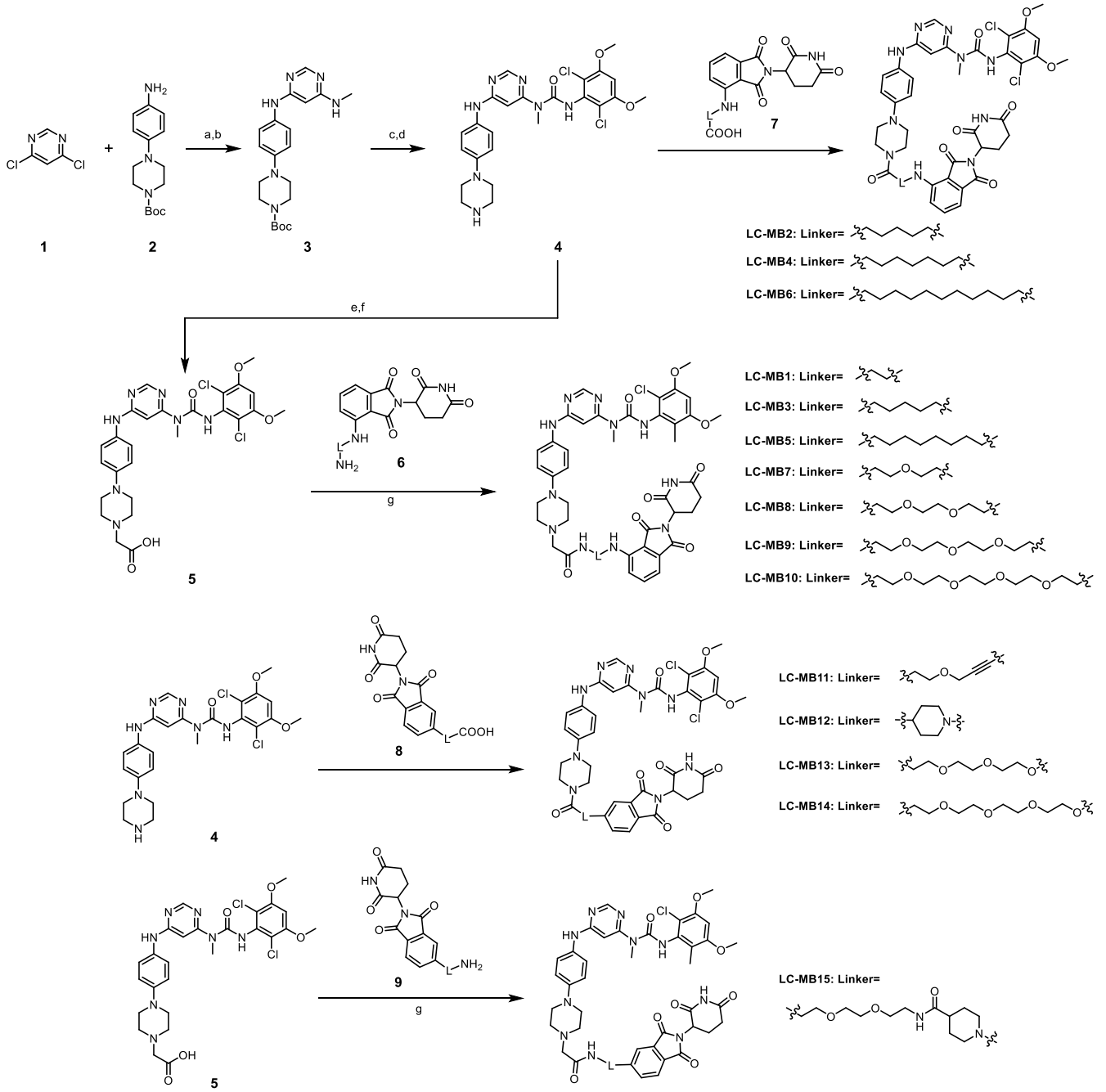

[a](a) i-PrOH, DIPEA, 40 °C; (b) 1-butanol, DIPEA, methylamine, 120 °C; (c) 2,6-dichloro-3,5-dimethoxyaniline, triphosgene, THF, triethylamine, 80 °C; (d) toluene, DIPEA, 80 °C; (e) *tert*-butyl bromoacetate, DMF, K_2CO_3; (f) DCM, TFA; (g) HATU, DIPEA, DMF, rt.

https://doi.org/10.1021/acs.jmedchem.3c00150
J. Med. Chem. XXXX, XXX, XXX−XXX

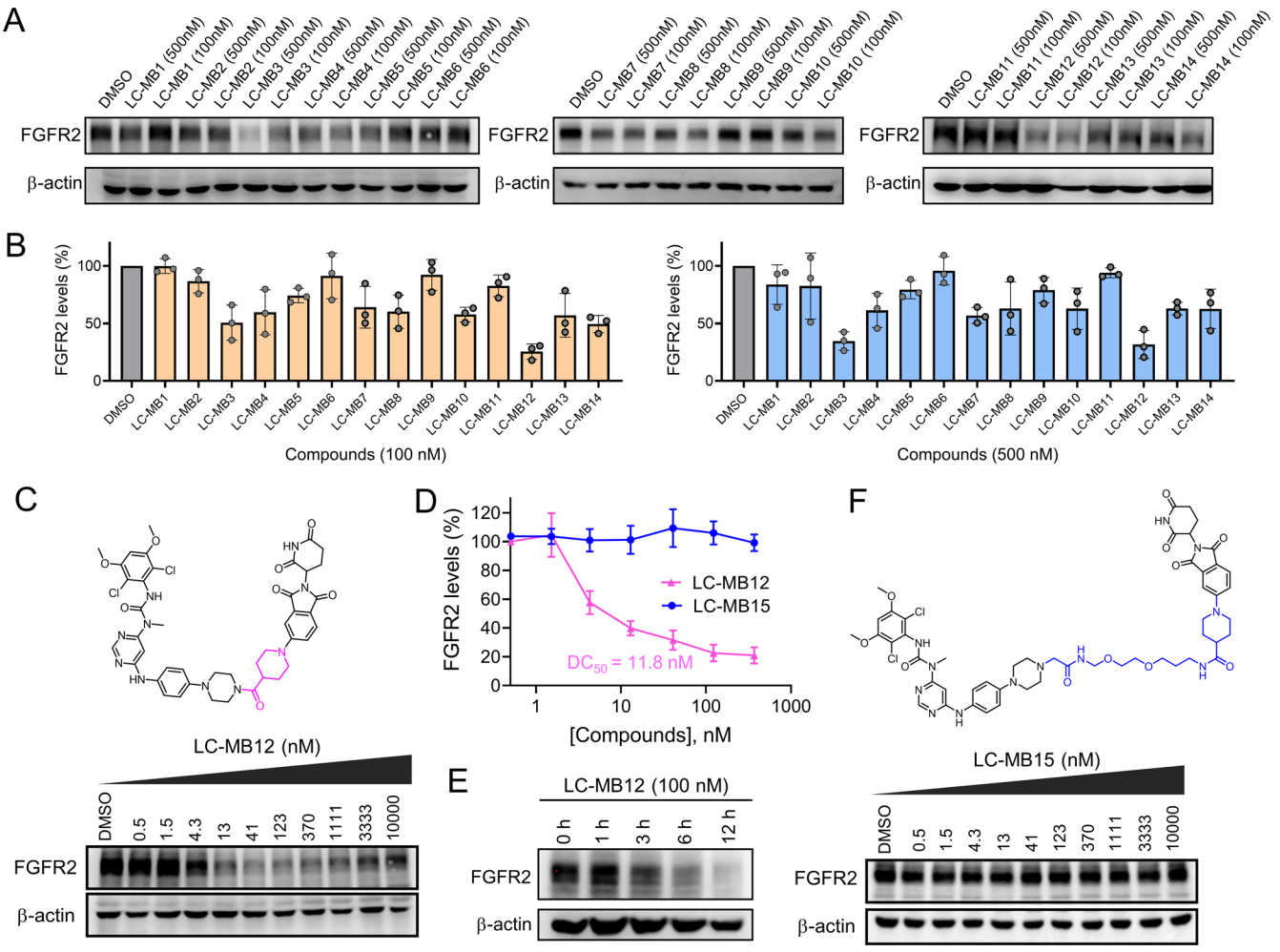

Figure 2. Identification of LC-MB12 as an efficient FGFR2 degrader. (A) Representative western blots evaluating the total FGFR2 levels in KATO III cells following treatment using the indicated PROTACs at 100 and 500 nM, or DMSO for 6 h. (B) Quantitative analysis of the relative FGFR2 level presented as the FGFR2/β−actin ratio and normalized to DMSO-treated cells. Data were obtained from three independent biological experiments. (C,D) Chemical structure of LC-MB12 and FGFR2 levels in KATO III cells after treatment with LC-MB12 (0.5−10,000 nM) for 6 h. (E) Time-course of FGFR2 degradation. (F) Chemical structure of LC-MB15 and FGFR2 levels in KATO III cells after treatment with LC-MB15 (0.5−10,000 nM) for 6 h.

resistant mutations such as N550K and K660M (FGFR2 numbering).[12] Meanwhile, the irreversible inhibitor futibatinib is effective against certain FGFR mutants. However, cancer cells may acquire secondary resistance to covalent inhibitors via cysteine residue mutations since this is commonly described in other irreversible RTK inhibitor-treated patients.[14] In addition, these developed FGFR-selective inhibitors are pan-FGFR inhibitors that can result in on-target toxic side effects mainly caused by FGFR1 inhibition. The "FGFR1-specific" toxicity profiles include hyperphosphatemia and tissue mineralization, which are likely related to the variation of endocrine FGF23 mediated signaling.[15] For instance, the most common treatment-emergent side effect in the phase I dose-expansion trial of futibatinib is hyperphosphatemia, which occurs in 81.2% of patients.[16] Developing subtype-selective inhibitors remains challenging owing to the high sequence homology within the intracellular kinase domains of FGFR1-3.

Proteolysis-targeting chimeras (PROTACs) are heterobifunctional molecules that induce ubiquitylation of the protein of interest (POI) and promote its degradation via the ubiquitin−proteasome system. This event-driven degrader can avoid mutation-related resistance owing to its unique degradation mechanism.[17] Moreover, several PROTAC molecules possess greater target selectivity than their parental warheads. For example, FGFR degrader DGY-09-192 is a dual degrader of subtypes FGFR1 and 2, but it has no degradation activity toward FGFR3 and 4.[18] Similar selectivity converting functions of heterobifunctional degraders were observed among BTK and CDKs.[19] Therefore, effective degradation requires additional factors rather than POI target engagement. Additionally, RTK-targeting PROTAC has various advantages over inhibition alone. For instance, degradation of EGFR, HER2, and c-MET results in greater inhibition of cell proliferation and a more sustained inhibition of downstream signaling responses compared to kinase inhibitors.[20]

The multiple advantages of this degradation-based approach inspired us to further study the development of FGFR2 degraders. This work synthesized and screened a series of degraders that couple BGJ398 and a CRBN binder, resulting in the identification of a potent and orally bioavailable FGFR2 degrader, LC-MB12. This novel degrader induces rapid and efficient degradation of FGFR2 while showing less degradation potency against other FGFR isoforms. LC-MB12 was more potent than the parental inhibitor, BGJ398 in vitro and in vivo.

https://doi.org/10.1021/acs.jmedchem.3c00150
J. Med. Chem. XXXX, XXX, XXX−XXX

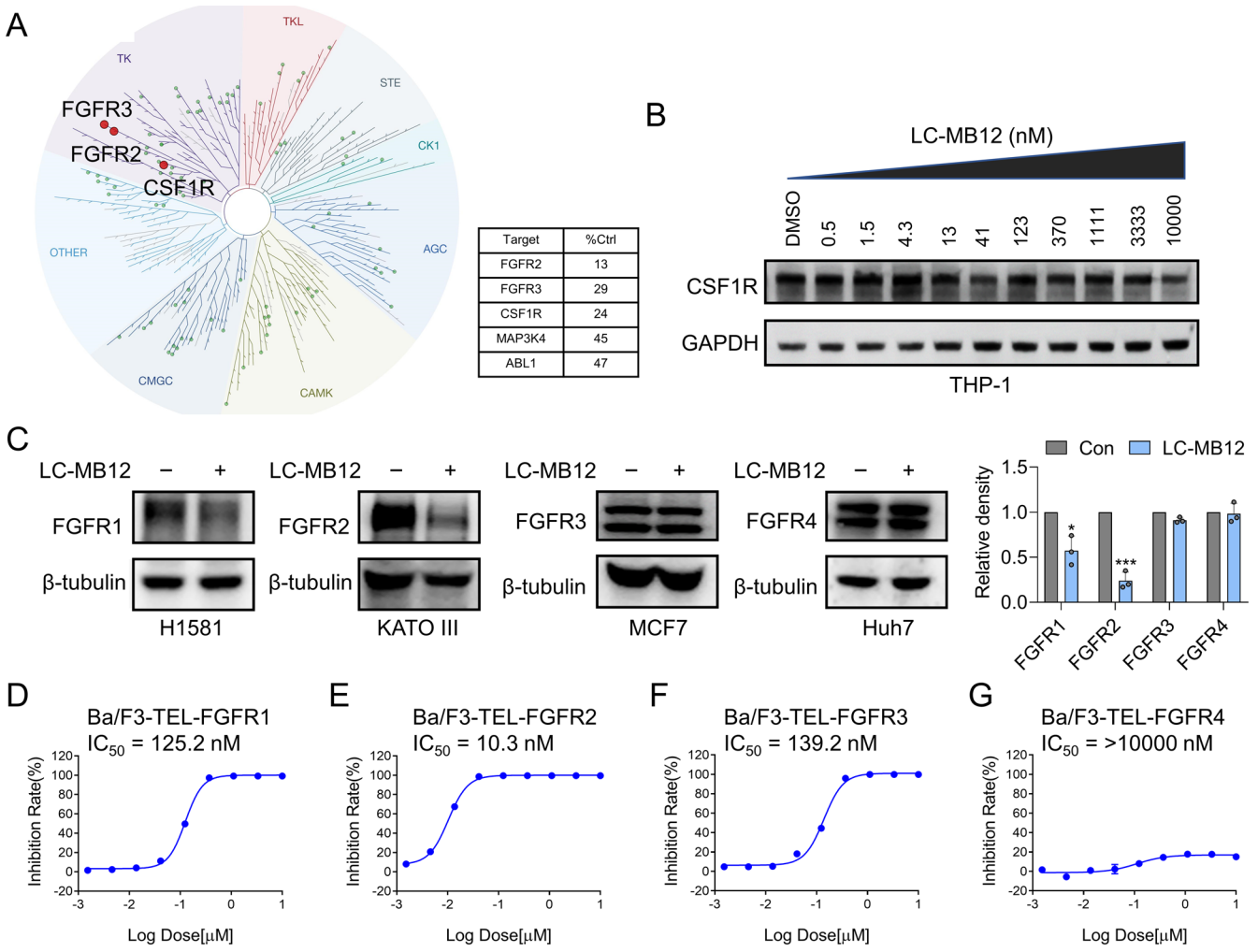

Figure 3. LC-MB12 is a selective degrader of FGFR2. (A) Selectivity profile of LC-MB12 against a 97-kinase panel (scanEDGE) tested at 1000 nM. (B) CSF1R levels in THP-1 cells after treatment with LC-MB12 (0.5−10,000 nM) for 6 h. (C) FGFR1, FGFR2, FGFR3, and FGFR4 levels in NCI-H1581, KATO III, MCF7, and Huh7 cells after treatment with 100 nM LC-MB12 for 6 h. Data were obtained from three biologically independent experiments. (D−G) Proliferation assay of LC-MB12 on four Ba/F3 cell lines stably expressing TEL-FGFR1−4. Ba/F3 cells were incubated with LC-MB12 for 72 h. Data were obtained from two biologically independent experiments.

This study provides a foundation for the development of therapeutic agents through targeted degradation of FGFR2.

2. RESULTS

2.1. Design and Optimization of FGFR Degraders. PROTAC molecules consist of a specific POI binder, an E3 ligase recruiter, and a linker tethering these two components in one molecule. Herein, we focused on the classic inhibitor BGJ398 (infigratinib) as an FGFR recruiter that selectively targets FGFR1−3. Analysis of the co-crystal structures of the BGJ398 bound FGFR1 kinase domain (PDB: 3TT0) indicated that the piperazine group was exposed to the solvent region; therefore, it could be utilized as a suitable linker tethering site (Figure 1A). Previously, a bivalent degrader (DGY-09-192) connecting BGJ398 to the von Hippel−Lindau (VHL) E3 ligase-recruiting ligand shows high potency in FGFR degradation that preferentially targets isoforms 1 and 2.[18] However, DGY-09-192 exhibits low oral bioavailability, with a F_{po} of 0.2%. Indeed, many VHL-based PROTACs have failed to achieve considerable oral exposure.[21]

In this study, thalidomide was chosen as the CRBN recruiter to expand the toolbox for FGFR degradation and achieve improved pharmacokinetic (PK) profiles. The crystal structures of the thalidomide-bound DDB1-CRBN E3 ubiquitin ligase complex show that the C4 and C5 positions of thalidomide are solvent-exposed and appropriate for PROTAC linkage.[22] In this study, two CRBN-targeting molecules were synthesized as novel candidate degraders by connecting to the piperazine site of BGJ398 (Figure 1B and Scheme 1), yielding LC-MB1 to LC-MB10 (C4 position) and LC-MB11 to LC-MB15 (C5 position). All the designed chimeras were synthesized by amide coupling or nucleophilic substitution incorporated via various linkers to the CRBN ligand. We systematically investigated the linker length, composition, and linker binding sites.

2.2. Degrader Screening and Identification of LC-MB12 as an Efficient FGFR2 Degrader. Next, we evaluated the efficacy of bifunctional molecules-induced FGFR2 degradation in a gastric cancer cell line, KATO III, which verified with relatively high basal FGFR2 expression levels. Treatment with 100 and 500 nM of each degrader resulted in different levels of FGFR2 protein degradation in KATO III after 6 h, according to western blotting (Figure 2A). Among the degraders with alkyl-based chain linkers and C4 position-

https://doi.org/10.1021/acs.jmedchem.3c00150
J. Med. Chem. XXXX, XXX, XXX−XXX

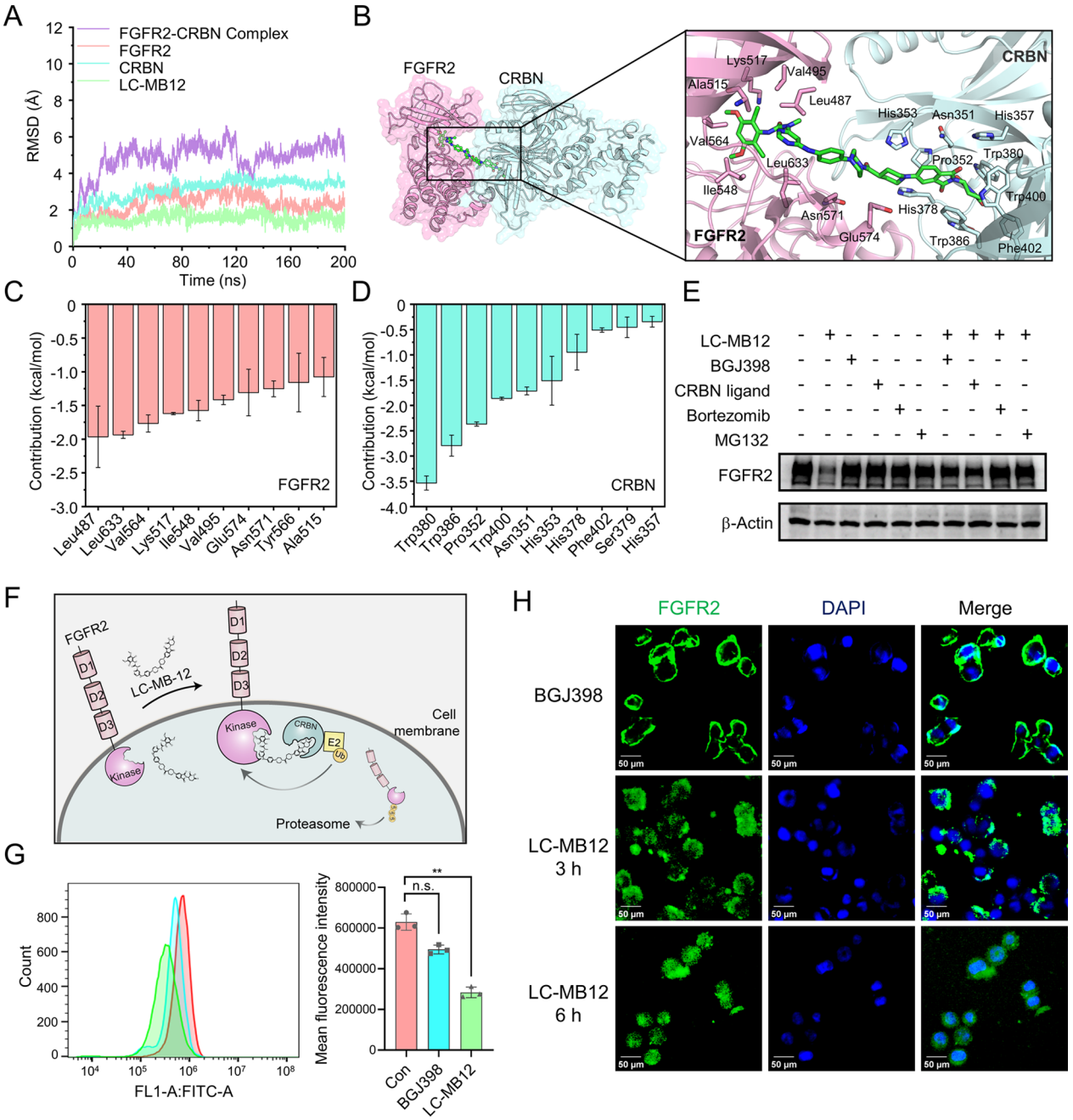

Figure 4. LC-MB12-mediated ternary complex formation and degradation of FGFR2 proteins. (A) Molecular modeling of the FGFR2-LC-MB12-CRBN ternary complex. RMSD curves for the FGFR2-CRBN complex, FGFR2-CRBN- PROTAC during 300 ns MD simulations. (B) Overview of the predicted ternary complex of FGFR2 (magenta), -CRBN (light blue), -PROTAC (green) extracted from 300 molecular dynamic (MD) simulations. A detailed view of the key residues is shown in the expanded view. (C) Key residues for the binding of PROTAC to FGFR2. (D) Key residues for the binding of PROTAC to CRBN. (E) Immunoblot of FGFR2 in KATO III cells pretreated with an excess amount (10 μM) of BGJ398, CRBN ligand, or 1 μM UPS inhibitor Bortezomib (Borte) or MG132, then treated with LC-MB12 (100 nM) for 6 h. (F) Schematic diagram showing the PROTAC molecule (LC-MB12) simultaneously engaged with membrane-bound FGFR2 and E3 ligase, and mediating FGFR2 ubiquitination and degradation through the ubiquitin/proteasome system. (G) Surface FGFR2 level of KATO III cells after BGJ398 or LC-MB12 treatment (100 nM/6 h) assessed by flow cytometry analysis. (H) Cellular localization of FGFR2 after treatment with BGJ398 or LC-MB12 (100 nM) for the indicated time. Scale bar, 50 μm.

linked thalidomide (LC-MB1~6), compounds with medium length of linker (LC-MB3 and LC-MB4) were found to be the most effective FGFR2 degraders, reducing the FGFR2 protein level by 66 and 40%, respectively, at 500 nM. Attempts to decrease (LC-MB1 and LC-MB2) or increase (LC-MB5 and LC-MB6) the alkyl linker length lowered the degradation rate. Notably, LC-MB1 and LC-MB6 had little or no effect on FGFR2 levels in KATO III cells.

The chemical composition of linkers may affect degradation potency.[23] Thus, another series of degraders was designed by substituting the alkyl chains into polyethylene glycol (PEG) linkers, yielding, LC-MB7 to LC-MB10 (Scheme 1). Surprisingly, four PROTACs with various lengths of PEG

https://doi.org/10.1021/acs.jmedchem.3c00150
J. Med. Chem. XXXX, XXX, XXX−XXX

embedded in the linker were less potent than degrader LC-MB3 (alkyl linker), with ~20−50% FGFR2 degradation after 500 nM/6 h treatment (Figure 2A,B).

Next, we evaluated the degraders LC-MB11 to LC-MB14, which incorporated type II CRBN binder (C5 position occupied by thalidomide). LC-MB11, LC-MB13, and LC-MB14 contain PEG units in their linkers and achieved modest FGFR2 degradation (Figure 2A,B). Interestingly, the introduction of a rigid piperidine group in the conjunction linker led to an effective degrader LC-MB12, which reduced FGFR2 protein by more than 70% at both 100 and 500 nM concentrations (Figure 2A,B).

To further distinguish the difference in potency, KATO III cells were treated with two promising active degraders (LC-MB3 and LC-MB12) at a broad concentration range (0.5−10,000 nM). The results showed LC-MB12 was characterized as the most potent degrader, with a DC_{50} (the degrader concentration that led to 50% protein degradation) of 11.8 nM and a maximal degradation (D_{max}) of ~80% after 6 h of treatment, while LC-MB3 showed a DC_{50} of 41.5 nM (Figures 2C,D and S1). Notably, affected by the "hook effect," weakened degradation potency was observed for LC-MB12 at concentrations above 300 nM, in which independent occupation of active degraders to FGFR2 and CRBN, thereby preventing the formation of ternary complex (Figure 2C). LC-MB12 also showed a strong time-dependent effect on degradation (Figure 2E), with a detectable reduction in FGFR2 levels after 3 h of treatment and ~90% degradation after 12 h.

To verify the importance of linker rigidity in LC-MB12, we performed further modifications by introducing a flexible PEG component while keeping the piperidine group identical to that in LC-MB12, yielding LC-MB15 (Figure 2F). The results showed that the introduction of the flexible PEG linker completely abolished the degradation potency of LC-MB12. Indeed, LC-MB15 had no obvious degradation activity at 10 μM.

In summary, among the degraders with alkyl-based chain linkers (LC-MB1−6), LC-MB3 having a nine atom-long carbon linker forms the most stable ternary complex for FGFR2 degradation. These results demonstrate that one atom modification in the linker can have a considerable influence on ternary complex formation. Compared with compounds LC-MB3 and LC-MB7, which with the same linker length but different compositions, PEG-based linker degrader (LC-MB7) showed much weaker degradation potency. While there is a great difference between linkers of the two active degraders, LC-MB3 and LC-MB12, the rigid linker of LC-MB12 may lead to a different three-dimensional conformation of the ternary complexes, thus serving as a key factor contributing to FGFR2 degradation. Our study demonstrates that linker length, composition, and rigidity work together to determine the potency of FGFR2 targeting degraders.

2.3. LC-MB12 Is a Selective Degrader of FGFR2. From a pharmacological viewpoint, target selectivity is a major characteristic of PROTAC molecules that prevents undesirable side effects. Thus, LC-MB12 was screened for additional profiling in vitro against a panel of 97 human protein kinases at 1000 nM to investigate possible interactions with other kinases. As shown in Figure 3A and Table S1, LC-MB12 retained comparable binding affinity for FGFR2 (87% inhibition rate) and FGFR3 (71% inhibition rate). This demonstrated that the linker attachment did not impede target binding. Only one off-target kinase was found among all the tested kinases, CSF1R (76% inhibition). To further clarify whether LC-MB12 also degrades off-target CSF1R, we treated THP-1 cells with different concentrations of LC-MB12. The result showed that LC-MB12 did not perturb CSF1R from 0.5 nM to 10 μM (Figure 3B). This demonstrates that kinase inhibition does not necessarily induce protein degradation and that FGFR remains the major binding target of LC-MB12.

The parental FGFR binder is an FGFR1-3 pan-inhibitor. Therefore, we next explored the degradation selectivity of LC-MB12 among the FGFR subfamily. Different cancer cells (NCI-H1581, KATO III, MCF7, and Huh7) that endogenously express the four isoforms of membrane-bound FGFRs were analyzed after 100 nM LC-MB12 treatment for 6 h (Figure 3C). Notably, LC-MB12 functioned as a highly selective degrader for FGFR2 (77% degradation rate in KATO III cells), while largely sparing FGFR1 with a 43% degradation rate in NCI-H1581 cells (Figures 3C and S2). In contrast, LC-MB12 failed to degrade FGFR3 and FGFR4 in MCF7 and Huh7 cells (Figure 3C).

To further assess the cellular activity of LC-MB12 and verify whether the selectivity in degradation impacts on cell proliferation, additional proliferation assays were conducted on four Ba/F3 cell lines stably expressing the TEL-FGFR1−4 fusion protein (cytoplasmic form). As shown in Figure 3D−G, Ba/F3 cells stably expressing TEL-FGFR2 were most sensitive to LC-MB12 treatment, with an IC_{50} of 10.3 nM. In contrast, Ba/F3 TEL-FGFR1 and TEL-FGFR3 cells were remarkably less sensitive to LC-MB12, with an IC_{50} of 125.2 and 139.2 nM, respectively. Interestingly, although LC-MB12 failed to degrade FGFR3 in MCF7 cells, it showed a modest growth inhibitory ability on Ba/F3 TEL-FGFR3 cells. This difference in potency may be caused by the different abundances of CRBN and the cellular localization distinction of FGFR2 between different cells. Consistent with the FGFR4 degradation results, LC-MB12 had no observed impact on the proliferation of cells overexpressing TEL-FGFR4. These results indicated that FGFR2 was the major downregulated protein in cells treated with LC-MB12 and confirmed the high selectivity of LC-MB12 for FGFR2.

2.4. LC-MB12 Mediates Ternary Complex Formation. Computational modeling was applied to gain more insight into the binding mode of the predicted ternary FGFR2−LCMB12−CRBN complex and provide clues for LC-MB12-mediated degradation using the PROTAC-Model method.[24] The predicted static ternary complex was optimized by performing 200 ns conventional molecular dynamics (MD) simulations (Figure 4A), followed by per-residue decompositions based on the MM/GBSA method. The root-mean-square deviations (RMSDs) of the protein backbone atoms (C_α) of the FGFR2-CRBN complex (FGFR2 and CRBN) tended to converge after approximately 75 ns of MD simulations. The RMSDs of the heavy atoms of LC-MB12 tended to converge after ~65 ns of MD simulations. These results indicated that the FGFR2-CRBN complex was quite stable after ~75 ns MD simulations and that LC-MB12 stably mediated ternary complex formation (Figure 4B). Stable MD simulation trajectories were then employed to predict the per-residue contribution to highlight the key residues for the binding of LC-MB12 to FGFR2 and CRBN (Figure 4C,D). The top 10-ranked residues for the binding of LC-MB12 to FGFR2 were Leu487, Leu633, Val564, Lys517, Ile548, Val495, Glu574, Asn571, Tyr566, and Ala515, while those for LC-MB12 to CRBN were Trp380, Trp386,

https://doi.org/10.1021/acs.jmedchem.3c00150
J. Med. Chem. XXXX, XXX, XXX−XXX

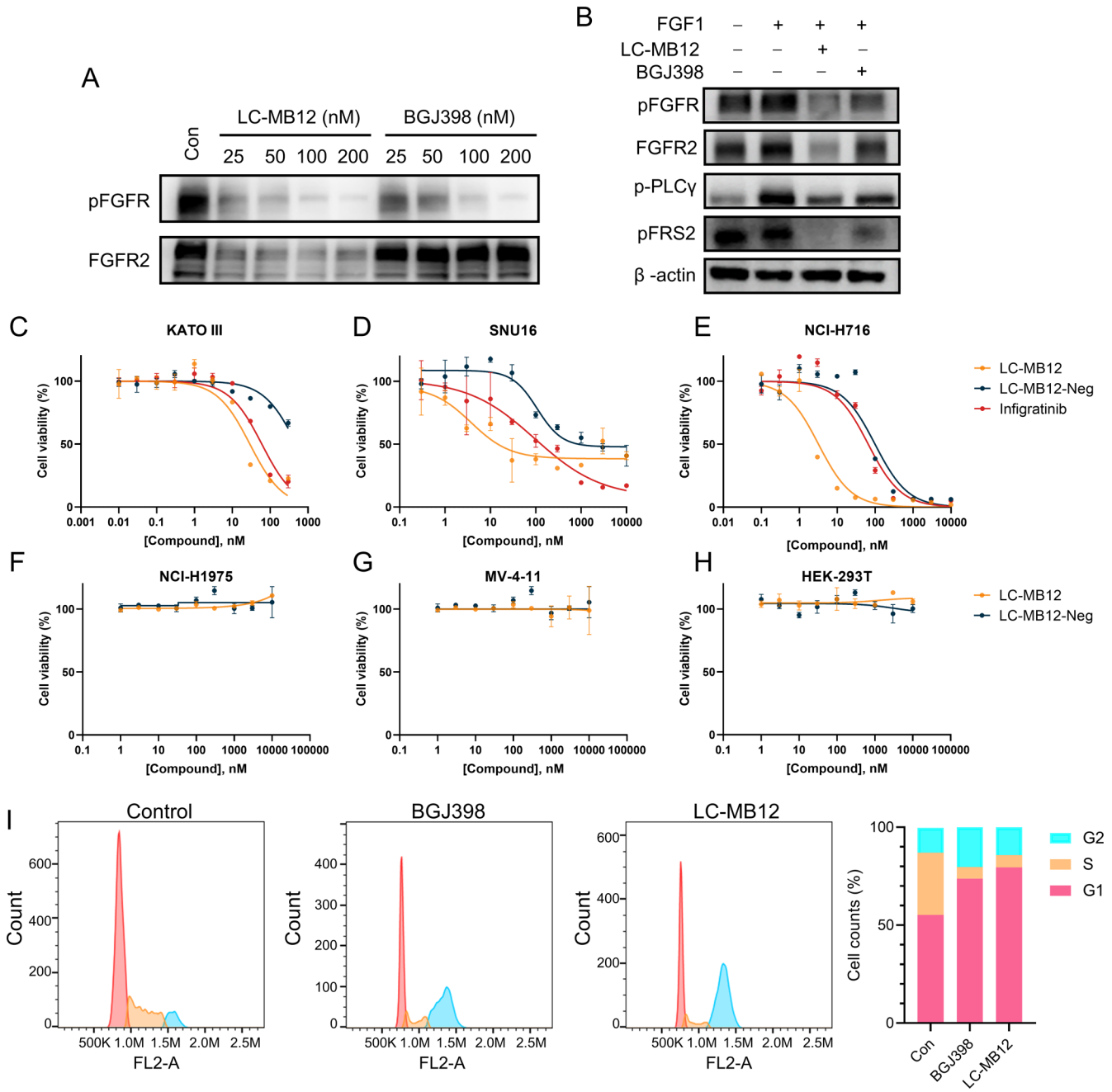

Figure 5. LC-MB12 inhibits the proliferation and FGFR2 signaling in cells. (A) Autophosphorylation level of FGFR2 on A-loop tyrosine residues monitored in KATO III cells after BGJ398 or LC-MB12 treatment for 6 h at the indicated concentrations. (B) Levels of pFGFR, pPLCγ, and pFRS2α in KATO III cells after 6 h of incubation with BGJ398 or LC-MB12 at 50 nM, then incubation with FGF1 for 10 min. (C–F) Proliferation assay of LC-MB12, LC-MB12-Neg, or BGJ398 on KATO III (C), SUN716 (D), NCI-H716 (E), NCI-H1975 (F), and MV-4-11 (G) cancer cells or HEK293T (H). Data were obtained from three independent biological experiments. (I) Cell cycle analysis of KATO III cells after treatment with BGJ398 or LC-MB12.

Pro352, Trp400, Asn351, His353, His378, Phe402, Ser379, and His357.

We then determined whether LC-MB12-mediated ubiquitination leads to FGFR2 degradation via the ubiquitin/proteasome system (UPS). As shown in Figure 4E, proteasome inhibitors bortezomib and MG132 completely abolished LC-MB12-induced FGFR2 degradation. This demonstrated that the degradation is proteasome-dependent. In addition, pretreatment with an excess amount of FGFR- or CRBN-binding ligand rescued FGFR2 degradation by LC-MB12. Meanwhile, LC-MB12-Neg, a negative control of LC-MB12, bearing methyl group at the glutarimide NH to reduce its binding affinity for CRBN, failed to induce LC-MB12 degradation (Figure S3). These results confirmed that FGFR2 degradation required the FGFR2–LC-MB12–CRBN ternary complex formation and proteasome degradation.

2.5. LC-MB12 Mediates the Degradation of Membrane-Bound FGFR2 Proteins. A large percentage of developed PROTACs target intracellular molecules.[25] Therefore, this study explored whether LC-MB12 directly eliminates the FGFR2 target from the cell membrane (Figure 4F). This hypothesis was tested by incubating KATO III cells with a 100

https://doi.org/10.1021/acs.jmedchem.3c00150
J. Med. Chem. XXXX, XXX, XXX–XXX

Table 1. Effect of LC-MB12 and LC-MB12-Neg on the Proliferation of Representive Cells[a]

	KATO III	SNU16	NCI-H716	NCI-H1975	MV-4-11	HEK293T
LC-MB12	29.1 ± 0.2	3.7 ± 2.9	3.2 ± 0.3	>10,000	>10000	>10000
LC-MB12-Neg	497.3 ± 32.8	107.6 ± 17.0	99.5 ± 2.0	>10,000	>10000	>10000
infigratinib	60.3 ± 2.1	95.4 ± 34.0	65.9 ± 4.6			

[a]The data are represented as the mean ± s.d.

Table 2. In Vivo PK Properties of LC-MB12

parameter	$T_{1/2}$	T_{max}	C_{max}	$AUC_{(0-\infty)}$	V_{ss}	CL	F
unit	h	h	ng/mL	h*ng/mL	mL/kg	mL/h/kg	%
iv (3 mg/kg)	0.97	0.083	655.29	421.61	6233.19	7289.12	
po (20 mg/kg)	1.47	2.67	82.07	387.27			13.07

nM BGJ398 inhibitor or LC-MB12 degrader for 6 h and analyzing FGFR2 levels by flow cytometry. LC-MB12 significantly reduced the amount of membrane-bound FGFR2 (Figure 4G). This indicated that LC-MB12-induced CRBN recruitment promoted FGFR2 ubiquitination, internalization, and subsequent degradation. In addition, immunofluorescence assays showed that FGFR2 was relocated from the cell membrane to intracellular vesicles compared to BGJ398 after the cells were treated with LC-MB12 for 3 or 6 h at 100 nM (Figure 4H). The 6 h LC-MB12 treatment induced marked receptor internalization and re-localization to the perinuclear section compared to the 3 h treatment. Together, these results provide evidence that LC-MB12 induces FGFR2-LC-MB12-CRBN ternary complex formation, thereby promoting the internalization of endogenous FGFR2 prior to degradation via the proteasome. Recruitment of the ubiquitin−proteasome machinery to the near cell membrane is feasible despite the fact that CRBN E3 ligases are cytosolic proteins.

2.6. LC-MB12 Inhibits the Proliferation of FGFR2-Amplified Cancer Cells and Blocks Downstream Signaling. We next assessed the functional consequences of LC-MB12-mediated degradation compared to those of FGFR inhibition by BGJ398 in cells. There was a robust FGFR autophosphorylation on the A-loop tyrosine (Tyr656/657) in the untreated KATO III cells (Figure 5A). FGFR A-loop phosphorylation was rapidly suppressed upon LC-MB12 treatment at the lowest degrader concentration (25 nM). In contrast, cells treated with the BGJ398 kinase inhibitor exhibited modest phosphorylation levels at 25 nM. In addition, the functional consequences of the LC-MB12 degrader on the phosphorylation of the two immediate downstream substrates of FGFR (PLCγ and FRS2) were evaluated (Figure 5B). Upon stimulation with the paracrine ligand FGF1, cells treated with LC-MB12 exhibited lower levels of FGFR, PLCγ, and FRS2 phosphorylation than those treated with the kinase inhibitor at 50 nM. This functional consequence is consistent with the ability of LC-MB12 to remove plasma membrane-bound FGFR2, thus enhancing the inhibitory effect of downstream signaling. Notably, the inhibition of phosphorylation levels of substrate FRS2 was more significant than PLCγ, in the LC-MB12 treated cells.

Since the proliferation of KATO III cells greatly relies on FGFR2 signaling, we next examined the anti-proliferative effects of LC-MB12 in this gastric cancer cell line. We found that the antiproliferative IC_{50} of LC-MB12 was 29.1 nM after 72 h of incubation (Figure 5C). In contrast, BGJ398 and LC-MB12-Neg exhibited 2- and 17-fold lower potency in the KATO III proliferation assay (IC_{50} = 60.3 and 497.3 nM, respectively). As shown in Figure 5D,E and Table 1, the IC_{50} of LC-MB12 in another FGFR2-amplified cancer (SNU16) was as low as 3.7 nM, which was 25- and 29-fold lower than that of BGJ398 and LC-MB12-Neg (IC_{50} = 95.3 and 107.6 nM, respectively). Similar results were observed in the FGFR2-overexpressed colorectal cancer cells (NCI-H716). In contrast, LC-MB12 and LC-MB12-Neg showed no significant inhibitory activity on NCI-H1975 (EGFR-driven) and MV-411 (FLT3-ITD-driven) cells or HEK293T with low FGFR2 expression (Figure 5F−H). Next, we used flow cytometry to study the effect of the compound on the cell cycle of KATO III cells. LC-MB12 exhibited a stronger effect in stopping the cell cycle, primarily in the G0/G1 phase (Figure 5I). Together, these results demonstrate the advantages of FGFR2 removal over inhibition of kinase activity.

2.7. LC-MB12 Is a Potent FGFR2 Degrader In Vivo. We next investigated the PK profile of LC-MB12 in mice to evaluate its suitability for further in vivo studies (Table 2). The LC-MB12 plasma concentrations were determined following a single-dose treatment of LC-MB12 via oral administration (PO, 20 mg/kg) or intravenous injection (IV, 3 mg/kg). LC-MB12 showed fast absorption after PO dosing, with C_{max} reached at 2.6 h. Acceptable plasma concentrations were observed and sustained at levels above the DC_{50} values of LC-MB12 during most of the experimental time course. Notably, LC-MB12 is orally bioavailable with F = 13%. Binding of compound LC-MB12 to plasma proteins was evaluated in dog, rat, and mouse plasma (Table S2), indicating compound LC-MB12 showed a high bound fraction in plasma. Further studies of LC-MB12 will focus on its pharmacodynamics and tissue distribution in vivo.

For the initial toxicological study, LC-MB12 was orally administered to mice for 30 days (20 mg/kg/day, n = 6). According to the Figure S4, no change in organ weight was observed between the vehicle-treated and LC-MB12-treated groups. Furthermore, LC-MB12 had no apparent hepatotoxicity or nephrotoxicity compared to the vehicle control, as determined by AST/ALT and creatinine assays. Additionally, hematoxylin and eosin staining analysis of the heart, liver, spleen, lung, and kidney showed no obvious morphological aberrations in organ tissues after LC-MB12 treatment. These observations suggest that LC-MB12 is well tolerated in vivo.

Next, LC-MB12 was selected for further in vivo evaluation given its low toxicity, excellent potency, and good PK profiles. SNU-16 was selected as an alternative FGFR2-dependent gastric cancer cell line[26] to assess the in vivo anti-cancer activity of LC-MB12 owing to the low success rate of KATO

https://doi.org/10.1021/acs.jmedchem.3c00150
J. Med. Chem. XXXX, XXX, XXX−XXX

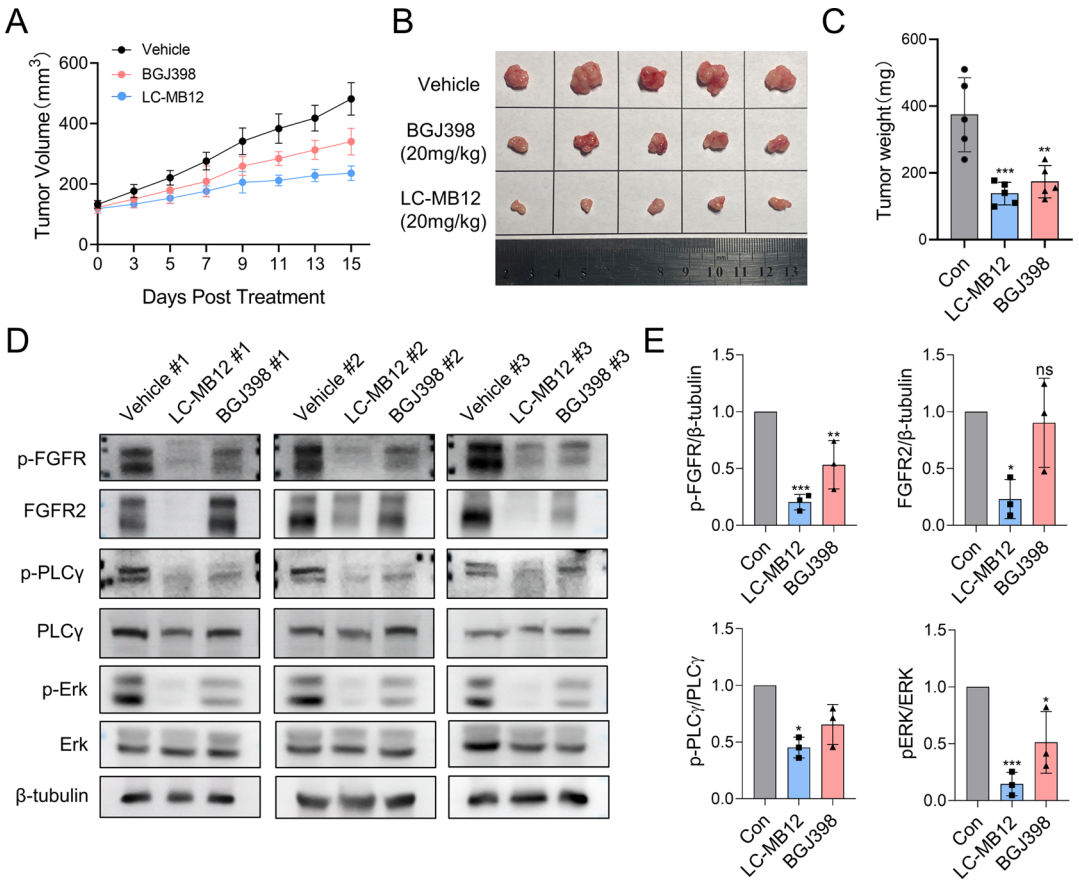

Figure 6. LC-MB12 is a potent FGFR2 degrader in vivo. (A) Antitumor efficacy of compounds LC-MB12 and BGJ398 in a SNU-16 xenograft model. SNU-16 tumor-bearing female BALB/c nude mice (n = 5) were treated with compound LC-MB12 and BGJ398, or vehicle at 20 mg/kg/day. Tumor sizes were recorded every 2−3 days. (B) Tumor images of each group after LC-MB12 and BGJ398, or vehicle treatment. (C) Tumor weights in each group after treatment with LC-MB12 and BGJ398, or vehicle. (D,E) Western blot analysis of tumor lysates for pFGFR, FGFR2, pPLCγ, and pErk levels.

III inoculation. SNU-16 tumor-bearing mice were administered LC-MB12 or BGJ398 (20 mg/kg, p.o., QD) for 15 d. LC-MB12 achieved 63.1% tumor growth inhibition in the SNU-16 xenograft model, while BGJ398 achieved 53.7% tumor growth inhibition (Figure 6A−C). A 20 mg/kg dose of LC-MB12 was well tolerated in mice, and no body weight loss was observed throughout the study (Figure S2). To test the effect of compound LC-MB12 on FGFR2 and downstream signaling in tissue, tumor samples were analyzed. It showed a significant reduction in FGFR phosphorylation and total FGFR2 protein levels and decreased phosphorylation levels of downstream pPLCγ and ERK1/2 (Figure 6D,E). Owning to the efficient degradation of FGFR2, LC-MB12 exhibited a stronger inhibitory effect on the FGFR2 signaling pathway than BGJ398. Thus, LC-MB12 is an efficient degrader and nontoxic in vivo and is a novel and promising candidate for gastric cancer treatment.

3. DISCUSSION AND CONCLUSIONS

FGFRs belong to a class of RTKs with four known members. The kinase domain of FGFR1-4 shares high sequence homology (>60%). Dysregulation of FGFR signaling results in many types of cancer. FGFR2 is frequently amplified or found with gene fusion in intrahepatic cholangiocarcinoma and gastric cancer.[6] Numerous efforts have been made to identify FGFR kinase inhibitors for the treatment of related cancers. However, these ATP-competitive inhibitors show dose-limiting toxicity that is mainly caused by FGFR1 inhibition. Currently, it is still challenging to identify specific isoform-selective inhibitors owing to their highly conserved kinase domains. Recently, only a few examples of FGFR2 selective inhibitors in the early stages have been reported.[27,28]

PROTAC technology has displayed incredible potential as a protein degradation strategy, with striking advantages compared to traditional inhibitors.[20] PROTAC-induced degradation requires the formation of ternary complexes, targeted ubiquitination, and degradation via the proteasome. We developed an LC-MB12 degrader that efficiently degraded FGFR2 at nanomolar concentrations (10 nM) in cells by tuning the linker length, composition, and spatial orientation of FGFR and E3 ligase in PROTAC conjugation. The rigid structure of LC-MB12 was a key factor contributing to FGFR2 degradation since the introduction of a flexible component into LC-MB12 abolished its degradation potency. Interestingly, a similar situation was recently observed in the development of FAK degrader.[29] Our study reinforces the significance of linker rigidity in the PROTAC design, and slight modifications can significantly affect the degradation process.

It is very difficult to discover isoform-selective inhibitors owing to the highly conserved RTK domain, especially in the FGFR subfamily. In addition, pan-FGFR kinase inhibitors can lead to undesirable toxicities. Meanwhile, the PROTAC method may achieve greater selectivity by adjusting factors such as E3 binders, linker length, composition, and rigidity.

https://doi.org/10.1021/acs.jmedchem.3c00150
J. Med. Chem. XXXX, XXX, XXX−XXX

Notably, although BGJ398 was identified as a conventional pan-FGFR kinase inhibitor, it was successfully transformed into a relatively isoform-selective degrader LC-MB12 for FGFR2, with less degradation potency for FGFR1, FGFR3, and FGFR4. LC-MB12 was bound to CSF1R in vitro. However, little or no CSF1R degradation was observed after LC-MB12 treatment at various concentrations. Thus, our findings verify that PROTAC transformation provides a promising strategy for converting multi-targeted inhibitors into selective or even isoform-selective degraders similar to that of other recently determined degraders: SMARCA2,[30] CDKs,[31] TRK,[32] and cMET.[33] However, the mechanism underlying the selective degradation of the FGFR2 isoform by LC-MB12 remains unclear. Notably, different E3 ubiquitin ligase-recruiting binders may have different target selectivity. Indeed, the VHL-recruiting FGFR degrader DGY-09-192[18] is a dual degrader of FGFR1 and 2, while CRBN- based PROTAC LC-MB12 was more selective for FGFR2. The different cooperative interactions between E3 and the targets may lead to a selectivity difference.[34]

PROTAC molecules demonstrate a greater and long-lasting effect than the parent inhibitors, leading to a stronger impact on the scaffolding function together with downstream signaling of the targets.[35] Indeed, the most potent degrader developed in this study (LC-MB12) was more effective at suppressing the phosphorylation of FGFR and downstream substrates (such as FRS2α) than the parent kinase inhibitor. In addition, LC-MB12 showed a 3-fold higher potency than BGJ398 against the proliferation of KATO III cells. Indeed, as a FGFR2 degrader, LC-MB12 abolished the kinase activity due to the reduced abundance of FGFR2. LC-MB12 probably disturbs the scaffolding function of FGFR (which normally forms the asymmetric transphosphorylating dimer demonstrated in our previous study[3]) and removes the docking site for the downstream signalosome, such as the FRS2/SHP2/Gab1/Grab2 complex. Attenuating the scaffolding role of FGFR2 may prevent the progression of compensatory feedback pathways. Finally, a common gap exists between the efficacy at the cell-based level and in vivo animal models based on the data of reported PROTACs. To our delight, this study showed that LC-MB12 provides good oral bioavailability and knockdown of FGFR2 protein in tumors based on PK data and xenograft mouse studies.

In summary, PROTAC technology has significantly boosted novel drug discovery programs; however, its application to degrade membrane-bound proteins such as RTKs is still in its early stages. We developed an efficient, isoform-selective, and orally bioavailable FGFR2 degrader through a comprehensive medicinal chemistry investigation and pharmacological evaluation: LC-MB12. We verified the ability to transform a pan-FGFR inhibitor into an FGFR2 selective and in vivo efficacious degrader. To the best of our knowledge, this is the first report of an orally bioavailable FGFR2 selective degrader. The FGFR2 degrader discovered in this study offers a new chemical tool for deciphering the biology of FGFR2 and provides a potential novel therapeutic choice for patients with tumors containing FGFR2 mutations.

4. EXPERIMENTAL SECTION

4.1. Chemistry. In general, commercial reagents including solvents and other chemicals were used without further purification. Reagents were purchased from Sigma-Aldrich, Aladdin, and Energy Chemical. All reactions were monitored by TLC. ^{1}H NMR and ^{13}C NMR spectra were determined on a Bruker 400 MHz instrument. Electron spray ionization mass spectra in positive mode (ESI-MS) results were collected on Waters Alliance (e2695) equipped with a QDa and PDA detector (2998). Chromatographic purification was done on Silica Gel 60. The purities of all the synthesized compounds were >95% determined using the analytical HPLC on a Shimadzu LC-20AD system equipped with a UV detector (SPD-20A) fitted with a Diamonsil C18 column (5 μm, 250 mm × 4.6 mm). The ^{1}H NMR and ^{13}C NMR spectra data and HPLC traces of the synthesized compounds are shown in Supporting Information.

4.1.1. tert-Butyl 4-(4-((6-(Methylamino)pyrimidin-4-yl)amino)-phenyl)piperazine-1-carboxylate (3). Step 1: 4,6-Dichloropyrimidine (1) (1.50 g, 11 mmol) and *N*,*N*-diisopropylethylamine (5.3 mL, 30 mmol) were added to isopropanol (30 mL) and stirred at room temperature. *tert*-Butyl 4-(4-aminophenyl)piperazine-1-carboxylate (2) (2.77 g, 10 mmol) dissolved in 10 mL of isopropanol was added dropwise at room temperature. The purple solution was then stirred at room temperature overnight. The reaction solution was filtered, and the solid product was washed with an appropriate amount of ethanol to afford the crude product as an off-white solid (3.2 g, 83%). Step 2: *tert*-Butyl 4-(4-((6-chloropyrimidin-4-yl)-amino)phenyl)piperazine-1-carboxylate (1.92 g, 5 mmol) was suspended in 1-butanol (15 mL) and DIPEA (2.8 mL, 15 mmol) was added, followed by 5 mL of methylamine (30−33 wt.% in methanol). The reaction vessel was then sealed, and the mixture was heated at 120 °C overnight. The solvent was evaporated to provide the title compound without further purification.

4.1.2. 3-(2,6-Dichloro-3,5-dimethoxyphenyl)-1-methyl-1-(6-((4-(piperazin-1-yl)phenyl)amino)pyrimidin-4-yl)urea (4). Step 1: 2,6-Dichloro-3,5-dimethoxyaniline (444 mg, 2.0 mmol) and triphosgene (297 mg, 1 mmol) were dissolved in THF (20 mL). At −10 °C, triethylamine (1.1 mL, 8 mmol) was slowly added, and a white precipitate formed as the reaction was slowly allowed to warm to room temperature. After 30 min of reaction, heated to 80 °C for reflux reaction for 1 h. Evaporation of the solvent gave a pale-yellow solid. Step 2: *tert*-butyl 4-(4-((6-(methylamino)pyrimidin-4-yl)amino)-phenyl)piperazine-1-carboxylat(3) (768 mg, 2 mmol) was added to the round-bottomed flask of Step 1, 30 mL of toluene was added to dissolve, DIPEA (1.5 mL, 8 mmol) was added, and the reaction was carried out at 80 °C overnight. The solvent was evaporated, and the crude product was purified by silica gel chromatography to afford the white solid (732 mg, 1.16 mmol, 58%). Step 3: *tert*-Butyl 4-(4-((6-(3-(2,6-dichloro-3,5-dimethoxyphenyl)-1,3-dimethylureido)pyrimidin-4-yl)amino)phenyl)piperazine-1-carboxylate (732 mg, 1.16 mmol) was dissolved in DCM (5 mL) and TFA (5 mL) was added. The solution was stirred for 2 h, and the solvent evaporated. The residue was then dissolved in THF and stirred with sat. aqueous $NaHCO_3$ for 30 min. The brown precipitate was then filtered, washed with water, and dried to provide the title compound as a yellow solid (542 mg, 1.02 mmol).

4.1.3. 2-(4-(4-((6-(3-(2,6-Dichloro-3,5-dimethoxyphenyl)-1,3-dimethylureido)pyrimidin-4-yl)amino)phenyl)piperazin-1-yl)acetic Acid (5). Step 1: 1-(2,6-Dichloro-3,5-dimethoxyphenyl)-1,3-dimethyl-3-(6-((4-(piperazin-1-yl)phenyl)amino)pyrimidin-4-yl)urea (4) (150 mg, 0.28) was dissolved in DMF (3 mL) and treated with K_2CO_3 (155 mg, 1.12 mmol). *T*-butyl bromoacetate was added (53 mg, 0.28 mmol), the mixture was stirred at room temperature overnight, and then water was added, followed by extraction with ethyl acetate. Combined extracts were washed with brine, dried with Na_2SO_4, and purified by silica gel chromatography to provide the *t*-butyl ester. Step 2: *tert*-Butyl 2-(4-(4-((6-(3-(2,6-dichloro-3,5-dimethoxyphenyl)-1,3-dimethylureido)pyrimidin-4-yl)amino)phenyl)piperazin-1-yl)acetate was then dissolved in DCM (2 mL) and TFA (2 mL) was added. The solution was stirred for 2 h, and the solvent was evaporated to provide the title compound (112 mg, 0.19 mmol, 68%). LC/MS *m*/*z*: calcd $[M + H]^+$, 590.16; found, 590.39.

4.1.4. 3-(2,6-Dichloro-3,5-dimethoxyphenyl)-1-(6-((4-(4-(1-(2-(2,6-dioxopiperidin-3-yl)-1,3-dioxoisoindolin-5-yl)piperidine-4-carbonyl)piperazin-1-yl)phenyl)amino)pyrimidin-4-yl)-1-methylurea (LC-MB12). 1-(2-(2,6-Dioxopiperidin-3-yl)-1,3-dioxoisoindolin-5-yl)piperidine-4-carboxylic acid (22 mg, 0.057 mmol), 3-(2,6-dichloro-

https://doi.org/10.1021/acs.jmedchem.3c00150
J. Med. Chem. XXXX, XXX, XXX−XXX

3,5-dimethoxyphenyl)-1-methyl-1-(6-((4-(piperazin-1-yl)phenyl)-amino)pyrimidin-4-yl)urea (4) (30 mg, 0.056 mmol), HATU (32 mg, 0.084 mmol), DIPEA(49 μL, 028 mmol), and DMF (1 mL) were added to a 10 mL round-bottomed flask. The reaction mixture was stirred at 25 °C for 1 h. The reaction mixture was diluted with water (30 mL), extracted with dichloromethane (20 mL × 3), washed with brine (30 mL × 3). The combined organic layer was dried over anhydrous Na_2SO_4, filtered, and concentrated to dryness under reduced pressure to afford the crude product, which was purified by chromatography on silica gel to give the desired product as a yellow powder (31 mg, 61%). ^{1}H NMR (400 MHz, Chloroform-*d*): δ 12.30 (s, 1H), 8.87 (s, 1H), 8.37 (s, 1H), 8.26 (s, 1H), 7.67 (d, *J* = 8.4 Hz, 1H), 7.26 (s, 3H), 7.06 (d, *J* = 8.6 Hz, 1H), 6.98 (d, *J* = 8.3 Hz, 2H), 6.52 (s, 1H), 6.13 (s, 1H), 4.94 (dd, *J* = 12.2, 5.3 Hz, 1H), 3.98 (d, *J* = 12.5 Hz, 2H), 3.91 (s, 6H), 3.77 (d, *J* = 33.2 Hz, 5H), 3.31 (s, 3H), 3.22 (d, *J* = 17.0 Hz, 5H), 3.06 (t, *J* = 12.1 Hz, 2H), 2.92−2.62 (m, 3H), 2.04−1.78 (m, 4H). ^{13}C NMR (101 MHz, Chloroform-*d*): δ 172.73, 171.52, 168.76, 168.09, 167.36, 160.90, 155.36, 154.72, 153.09, 134.90, 134.47, 125.56, 125.30, 119.29, 118.19, 117.69, 114.01, 108.86, 96.13, 77.36, 56.79, 49.26, 47.48, 37.89, 32.45, 31.58, 27.98, 22.88. LC−MS (ESI$^+$): calcd for $C_{43}H_{45}Cl_2N_{10}O_8$ [M + H]$^+$, 899.27; found, 899.47. HPLC t_R = 29.979 min (96.36% purity).

4.1.5. 2-(4-(4-((6-(3-(2,6-Dichloro-3,5-dimethoxyphenyl)-1-methylureido)pyrimidin-4-yl)amino)phenyl)piperazin-1-yl)-N-(2-((2-(2,6-dioxopiperidin-3-yl)-1,3-dioxoisoindolin-4-yl)amino)ethyl)-acetamide (LC-MB1). 2-(4-(4-((6-(3-(2,6-Dichloro-3,5-dimethoxyphenyl)-1-methylureido)pyrimidin-4-yl)amino)phenyl)piperazin-1-yl)acetic acid (5) (50 mg, 0.085 mmol), 4-((2-aminoethyl)amino)-2-(2,6-dioxopiperidin-3-yl)isoindoline-1,3-dione (27 mg, 0.085 mmol), HATU (49 mg, 0.13 mmol), DIPEA (75 μL, 0.43 mmol), and DMF (1.5 mL) were added to a 10 mL round-bottomed flask. The reaction mixture was stirred at 25 °C for 1 h. The reaction mixture was diluted with water (30 mL), extracted with dichloromethane (20 mL × 3), and washed with brine (30 mL × 3). The combined organic layer was dried over anhydrous Na_2SO_4, filtered, and concentrated to dryness under reduced pressure to afford the crude product, which was purified by chromatography on silica gel to give the desired product as a yellow-green powder (45 mg, 59%). ^{1}H NMR (400 MHz, DMSO-d_6): δ 12.08 (s, 1H), 11.13 (s, 1H), 9.48 (s, 1H), 8.40 (s, 1H), 7.64−7.53 (m, 1H), 7.42 (d, *J* = 8.4 Hz, 2H), 7.21 (dd, *J* = 15.5, 6.0 Hz, 1H), 7.03 (dd, *J* = 16.0, 7.0 Hz, 1H), 6.91 (d, *J* = 7.2 Hz, 4H), 6.73 (q, *J* = 6.1 Hz, 1H), 6.42 (s, 1H), 5.06 (dd, *J* = 12.9, 5.4 Hz, 1H), 3.94 (s, 6H), 3.31 (s, 3H), 3.20−2.79 (m, 6H), 2.71−2.31 (m, 12H). ^{13}C NMR (101 MHz, DMSO-d_6): δ 173.32, 170.59, 156.39, 154.71, 153.35, 136.73, 135.01, 132.68, 116.41, 113.06, 97.09, 57.18, 48.98, 40.55, 40.34, 40.13, 39.92, 39.71, 39.51, 39.30, 32.18. LC−MS (ESI$^+$): calcd for $C_{41}H_{44}Cl_2N_{11}O_8$ [M + H]$^+$, 888.27; found, 888.34. HPLC t_R = 31.241 min (97.94% purity).

4.1.6. 3-(2,6-Dichloro-3,5-dimethoxyphenyl)-1-(6-((4-(4-(6-((2-(2,6-dioxopiperidin-3-yl)-1,3-dioxoisoindolin-4-yl)amino)-hexanoyl)piperazin-1-yl)phenyl)amino)pyrimidin-4-yl)-1-methylurea (LC-MB2). Compound LC-MB2 was synthesized in a similar manner as the bispecific compound LC-MB12, yellow-green powder (64%). ^{1}H NMR (400 MHz, chloroform-*d*): δ 12.54 (s, 1H), 9.22 (s, 1H), 8.37 (s, 1H), 7.68 (s, 1H), 7.47 (t, *J* = 7.8 Hz, 1H), 7.23 (d, *J* = 7.6 Hz, 2H), 7.07 (d, *J* = 7.1 Hz, 1H), 6.96 (d, *J* = 8.4 Hz, 2H), 6.87 (d, *J* = 8.6 Hz, 1H), 6.50 (s, 1H), 6.22 (t, *J* = 5.6 Hz, 1H), 6.11 (s, 1H), 4.90 (dd, *J* = 11.9, 5.3 Hz, 1H), 3.90 (s, 6H), 3.79 (q, *J* = 4.3 Hz, 2H), 3.64 (t, *J* = 5.0 Hz, 2H), 3.28 (d, *J* = 10.9 Hz, 5H), 3.17 (s, 4H), 2.92−2.63 (m, 4H), 2.39 (t, *J* = 7.4 Hz, 2H), 1.71 (h, *J* = 7.2 Hz, 4H), 1.49 (q, *J* = 8.0, 7.6 Hz, 2H). ^{13}C NMR (101 MHz, Chloroform-*d*): δ 171.71, 171.40, 169.66, 168.94, 167.74, 154.63, 153.35, 147.01, 136.29, 135.01, 132.54, 116.76, 113.91, 111.56, 109.91, 95.87, 77.36, 56.74, 48.93, 42.48, 33.09, 32.26, 31.54, 29.16, 26.83, 24.97, 22.93. LC−MS (ESI$^+$): calcd for $C_{43}H_{47}Cl_2N_{10}O_8$ [M + H]$^+$, 901.29; found, 901.33. HPLC t_R = 31.351 min (98.96% purity).

4.1.7. 2-(4-(4-((6-(3-(2,6-Dichloro-3,5-dimethoxyphenyl)-1-methylureido)pyrimidin-4-yl)amino)phenyl)piperazin-1-yl)-N-(5-((2-(2,6-dioxopiperidin-3-yl)-1,3-dioxoisoindolin-4-yl)amino)-pentyl)acetamide (LC-MB3). Compound LC-MB3 was synthesized in a similar manner as the bispecific compound LC-MB1, yellow-green powder (58%). ^{1}H NMR (400 MHz, chloroform-*d*): δ 12.61 (s, 1H), 8.93 (s, 1H), 8.36 (s, 1H), 7.48 (t, *J* = 7.8 Hz, 1H), 7.20 (t, *J* = 7.4 Hz, 3H), 7.08 (d, *J* = 7.1 Hz, 1H), 6.95 (t, *J* = 6.1 Hz, 3H), 6.87 (d, *J* = 8.5 Hz, 1H), 6.51 (s, 1H), 6.22 (t, *J* = 5.6 Hz, 1H), 6.09 (s, 1H), 4.89 (dd, *J* = 12.0, 5.3 Hz, 1H), 3.91 (s, 6H), 3.37−3.18 (m, 11H), 3.08 (s, 2H), 2.91−2.62 (m, 8H), 1.77−1.38 (m, 6H). ^{13}C NMR (101 MHz, Chloroform-*d*): δ 171.38, 169.92, 169.55, 168.65, 167.60, 163.00, 160.79, 155.91, 154.57, 153.33, 149.08, 146.91, 136.20, 135.06, 132.49, 129.62, 125.19, 116.97, 116.61, 113.96, 111.55, 109.96, 95.89, 77.36, 77.25, 77.05, 76.73, 56.67, 53.47, 49.30, 48.88, 42.48, 38.72, 32.09, 31.44, 29.56, 28.90, 24.31, 22.83, 22.67. LC−MS (ESI$^+$): calcd for $C_{44}H_{50}Cl_2N_{11}O_8$ [M + H]$^+$, 930.31; found, 930.39. HPLC t_R = 32.209 min (98.40% purity).

4.1.8. 3-(2,6-Dichloro-3,5-dimethoxyphenyl)-1-(6-((4-(4-(8-((2-(2,6-dioxopiperidin-3-yl)-1,3-dioxoisoindolin-4-yl)amino)octanoyl)-piperazin-1-yl)phenyl)amino)pyrimidin-4-yl)-1-methylurea (LC-MB4). Compound LC-MB4 was synthesized in a similar manner as the bispecific compound LC-MB12, yellow-green powder (72%). ^{1}H NMR (400 MHz, chloroform-*d*): δ 12.58 (s, 1H), 9.43 (s, 1H), 8.37 (s, 1H), 7.70 (s, 1H), 7.47 (t, *J* = 7.8 Hz, 1H), 7.23 (d, *J* = 8.5 Hz, 2H), 7.06 (d, *J* = 7.1 Hz, 1H), 6.95 (d, *J* = 8.4 Hz, 2H), 6.86 (d, *J* = 8.5 Hz, 1H), 6.50 (s, 1H), 6.21 (t, *J* = 5.6 Hz, 1H), 6.11 (s, 1H), 4.90 (dd, *J* = 11.9, 5.4 Hz, 1H), 3.90 (s, 6H), 3.78 (m, 2H), 3.63 (t, *J* = 5.1 Hz, 2H), 3.29 (s, 3H), 3.27−3.10 (m, 6H), 2.91−2.65 (m, 3H), 2.37 (t, *J* = 7.6 Hz, 2H), 1.65 (t, *J* = 7.3 Hz, 4H), 1.39 (m, 7H). ^{13}C NMR (101 MHz, Chloroform-*d*): δ 171.82, 171.77, 169.64, 169.03, 167.77, 154.62, 153.40, 147.05, 136.23, 135.04, 132.53, 125.01, 117.65, 116.76, 113.91, 111.47, 109.86, 95.85, 77.36, 56.73, 48.92, 42.68, 33.34, 32.21, 31.53, 29.40, 29.22, 26.86, 25.27, 22.93. LC−MS (ESI$^+$): calcd for $C_{45}H_{51}Cl_2N_{10}O_8$ [M + H]$^+$, 929.32; found, 929.46. HPLC t_R = 32.536 min (97.68% purity).

4.1.9. 2-(4-(4-((6-(3-(2,6-Dichloro-3,5-dimethoxyphenyl)-1-methylureido)pyrimidin-4-yl)amino)phenyl)piperazin-1-yl)-N-(8-((2-(2,6-dioxopiperidin-3-yl)-1,3-dioxoisoindolin-4-yl)amino)octyl)-acetamide (LC-MB5). Compound LC-MB5 was synthesized in a similar manner as the bispecific compound LC-MB1, yellow-green powder (59%) .^{1}H NMR (400 MHz, chloroform-*d*): δ 12.61 (s, 1H), 9.45 (s, 1H), 8.36 (s, 1H), 7.59 (s, 1H), 7.48 (dd, *J* = 8.5, 7.1 Hz, 1H), 7.24−7.14 (m, 3H), 7.07 (d, *J* = 7.1 Hz, 1H), 6.94 (d, *J* = 8.9 Hz, 2H), 6.86 (d, *J* = 8.6 Hz, 1H), 6.52 (s, 1H), 6.22 (t, *J* = 5.6 Hz, 1H), 6.10 (s, 1H), 4.91 (dd, *J* = 12.0, 5.4 Hz, 1H), 3.91 (s, 6H), 3.34−3.18 (m, 12H), 3.08 (s, 2H), 2.92−2.62 (m, 8H), 1.64 (t, *J* = 7.3 Hz, 2H), 1.57−1.48 (m, 2H), 1.43−1.28 (m, 7H). ^{13}C NMR (101 MHz, Chloroform-*d*): δ 171.48, 169.84, 169.57, 169.13, 167.68, 162.92, 160.81, 155.77, 154.56, 153.33, 149.12, 146.97, 136.12, 135.03, 132.51, 129.68, 125.16, 116.96, 116.64, 113.94, 111.41, 109.88, 95.87, 86.79, 77.37, 77.26, 77.05, 76.74, 61.48, 56.67, 53.42, 49.43, 48.89, 42.62, 38.89, 32.10, 31.48, 29.56, 29.28, 29.12, 26.90, 26.86, 22.87, 14.16. LC−MS (ESI$^+$): calcd for $C_{47}H_{55}Cl_2N_{11}O_8Na$ [M + N]$^+$, 994.36; found, 994.51. HPLC t_R = 32.205 min (98.51% purity).

4.1.10. 3-(2,6-Dichloro-3,5-dimethoxyphenyl)-1-(6-((4-(4-(12-((2-(2,6-dioxopiperidin-3-yl)-1,3-dioxoisoindolin-4-yl)amino)-dodecanoyl)piperazin-1-yl)phenyl)amino)pyrimidin-4-yl)-1-methylurea (LC-MB6). Compound LC-MB6 was synthesized in a similar manner as the bispecific compound LC-MB12, yellow-green powder (54%).^{1}H NMR (400 MHz, chloroform-*d*): δ 12.54 (s, 1H), 9.51 (s, 1H), 8.37 (d, *J* = 4.7 Hz, 1H), 7.71 (s, 1H), 7.52−7.39 (m, 1H), 7.24 (d, *J* = 8.1 Hz, 2H), 7.05 (dd, *J* = 15.7, 7.1 Hz, 1H), 6.97 (d, *J* = 8.1 Hz, 2H), 6.85 (dd, *J* = 16.2, 8.5 Hz, 1H), 6.51 (s, 1H), 6.23 (m, 1H), 6.11 (s, 1H), 4.91 (dd, *J* = 12.1, 5.3 Hz, 1H), 3.91 (s, 6H), 3.80 (t, *J* = 5.3 Hz, 2H), 3.65 (t, *J* = 5.1 Hz, 2H), 3.30 (s, 3H), 3.27−3.08 (m, 5H), 2.92−2.69 (m, 2H), 2.37 (t, *J* = 7.6 Hz, 2H), 1.64 (t, *J* = 7.4 Hz, 4H), 1.42−1.16 (m, 17H). ^{13}C NMR (101 MHz, Chloroform-*d*): δ 171.95, 171.70, 169.62, 169.14, 167.80, 154.64, 153.35, 147.09, 136.21, 135.02, 132.56, 117.63, 116.76, 113.94, 111.42, 109.85, 95.89, 77.36, 56.75, 48.93, 42.73, 33.40, 32.25, 31.58, 29.61, 29.53, 29.38, 29.30, 27.01, 25.53, 22.93. LC−MS (ESI$^+$): calcd for $C_{49}H_{58}Cl_2N_{10}O_8Na$ [M + Na]$^+$, 1007.38; found, 1007.44. HPLC t_R = 31.199 min (98.72% purity).

https://doi.org/10.1021/acs.jmedchem.3c00150
J. Med. Chem. XXXX, XXX, XXX−XXX

4.1.11. 2-(4-(4-((6-(3-(2,6-Dichloro-3,5-dimethoxyphenyl)-1-methylureido)pyrimidin-4-yl)amino)phenyl)piperazin-1-yl)-N-(2-(2-((2-(2,6-dioxopiperidin-3-yl)-1,3-dioxoisoindolin-4-yl)amino)-ethoxy)ethyl)acetamide (LC-MB7). Compound LC-MB7 was synthesized in a similar manner as the bispecific compound LC-MB1, yellow-green powder (62%). ^{1}H NMR (400 MHz, chloroform-*d*): δ 12.59 (s, 1H), 9.28 (s, 1H), 8.36 (s, 1H), 7.47 (t, *J* = 7.8 Hz, 2H), 7.31 (s, 1H), 7.18 (d, *J* = 8.4 Hz, 2H), 7.08 (d, *J* = 7.1 Hz, 1H), 6.88 (d, *J* = 8.4 Hz, 3H), 6.50 (d, *J* = 11.0 Hz, 1H), 6.46 (t, *J* = 5.6 Hz, 1H), 6.09 (s, 1H), 4.89 (dd, *J* = 11.6, 5.6 Hz, 1H), 3.91 (s, 6H), 3.71 (t, *J* = 5.3 Hz, 2H), 3.61 (t, *J* = 5.1 Hz, 2H), 3.52 (q, *J* = 5.3 Hz, 2H), 3.45 (q, *J* = 5.3 Hz, 2H), 3.29 (s, 3H), 3.24−3.07 (m, 7H), 2.92−2.61 (m, 7H). ^{13}C NMR (101 MHz, Chloroform-*d*): δ 171.67, 169.59, 168.98, 167.64, 154.70, 153.46, 146.85, 136.32, 135.21, 132.62, 125.16, 117.15, 116.83, 114.13, 112.02, 110.51, 96.08, 77.36, 70.00, 69.26, 56.80, 53.18, 49.04, 42.59, 38.94, 32.22, 31.54, 22.94. LC−MS (ESI$^+$): calcd for $C_{43}H_{48}Cl_2N_{11}O_9$ [M + H]$^+$, 932.29; found, 932.39. HPLC t_R = 25.489 min (95.05% purity).

4.1.12. 2-(4-(4-((6-(3-(2,6-Dichloro-3,5-dimethoxyphenyl)-1-methylureido)pyrimidin-4-yl)amino)phenyl)piperazin-1-yl)-N-(2-(2-(2-((2-(2,6-dioxopiperidin-3-yl)-1,3-dioxoisoindolin-4-yl)amino)-ethoxy)ethoxy)ethyl)acetamide (LC-MB8). Compound LC-MB8 was synthesized in a similar manner as the bispecific compound LC-MB1, yellow-green powder (55%). ^{1}H NMR (400 MHz, chloroform-*d*): δ 12.61 (s, 1H), 9.88 (s, 1H), 8.36 (s, 1H), 7.64 (s, 1H), 7.46 (dd, *J* = 14.8, 7.1 Hz, 2H), 7.19 (d, *J* = 8.4 Hz, 2H), 7.08 (d, *J* = 7.1 Hz, 1H), 6.88 (dd, *J* = 18.7, 8.4 Hz, 3H), 6.51 (s, 1H), 6.42 (t, *J* = 5.6 Hz, 1H), 6.10 (s, 1H), 4.92 (dd, 1H), 3.91 (s, 6H), 3.71−3.63 (m, 6H), 3.61 (t, *J* = 5.1 Hz, 2H), 3.51 (q, *J* = 5.4 Hz, 2H), 3.41 (q, *J* = 5.7 Hz, 2H), 3.29 (s, 3H), 3.20 (d, *J* = 25.9 Hz, 6H), 2.90−2.68 (m, 8H). ^{13}C NMR (101 MHz, Chloroform-*d*): δ 171.76, 169.52, 167.70, 154.66, 153.44, 146.75, 136.25, 135.14, 132.64, 116.75, 114.01, 111.91, 110.43, 95.93, 77.48, 77.36, 77.16, 76.84, 70.92, 70.23, 70.01, 69.35, 56.77, 49.02, 42.28, 38.98, 32.20, 31.54, 23.13. LC−MS (ESI$^+$): calcd for $C_{45}H_{52}Cl_2N_{11}O_{10}$ [M + H]$^+$, 976.32; found, 976.32. HPLC t_R = 25.674 min (95.44% purity).

4.1.13. 2-(4-(4-((6-(3-(2,6-Dichloro-3,5-dimethoxyphenyl)-1-methylureido)pyrimidin-4-yl)amino)phenyl)piperazin-1-yl)-N-(2-(2-(2-(2-((2-(2,6-dioxopiperidin-3-yl)-1,3-dioxoisoindolin-4-yl)amino)-ethoxy)ethoxy)ethoxy)ethyl)acetamide (LC-MB9). Compound LC-MB9 was synthesized in a similar manner as the bispecific compound LC-MB1, yellow-green powder (54%). ^{1}H NMR (400 MHz, chloroform-*d*): δ 12.61 (s, 1H), 9.96 (s, 1H), 8.37 (d, *J* = 4.4 Hz, 1H), 7.57−7.43 (m, 2H), 7.21 (d, *J* = 8.8 Hz, 2H), 7.09 (d, *J* = 7.1 Hz, 1H), 6.91 (dd, *J* = 21.8, 8.6 Hz, 4H), 6.52 (s, 1H), 6.43 (t, *J* = 5.4 Hz, 1H), 6.10 (s, 1H), 4.92 (dd, *J* = 11.6, 5.4 Hz, 1H), 3.92 (s, 6H), 3.71−3.54 (m, 13H), 3.50 (d, *J* = 5.4 Hz, 2H), 3.43 (q, *J* = 5.5 Hz, 2H), 3.32−3.27 (m, 10H), 3.03−2.63 (m, 6H). ^{13}C NMR (101 MHz, Chloroform-*d*): δ 171.65, 169.41, 169.37, 167.64, 162.81, 160.75, 155.71, 154.58, 153.31, 146.76, 136.06, 135.06, 132.51, 124.97, 117.09, 116.77, 114.00, 111.71, 110.28, 95.96, 77.36, 77.04, 76.73, 70.73, 70.64, 70.49, 70.30, 69.82, 69.50, 56.68, 53.17, 49.03, 48.91, 42.40, 38.81, 32.09, 31.93, 31.48, 29.70, 29.36, 22.86, 22.69. LC−MS (ESI$^+$): calcd for $C_{47}H_{56}Cl_2N_{11}O_{11}$ [M + H]$^+$, 1020.35; found, 1020.31. HPLC t_R = 31.026 min (98.30% purity).

4.1.14. 2-(4-(4-((6-(3-(2,6-Dichloro-3,5-dimethoxyphenyl)-1-methylureido)pyrimidin-4-yl)amino)phenyl)piperazin-1-yl)-N-(14-((2-(2,6-dioxopiperidin-3-yl)-1,3-dioxoisoindolin-4-yl)amino)-3,6,9,12-tetraoxatetradecyl)acetamide (LC-MB10). Compound LC-MB10 was synthesized in a similar manner as the bispecific compound LC-MB1, yellow-green powder (52%). ^{1}H NMR (400 MHz, chloroform-*d*): δ 12.53 (s, 1H), 9.75 (s, 1H), 8.31 (s, 1H), 7.59 (s, 1H), 7.47 (s, 1H), 7.40 (dd, *J* = 8.5, 7.1 Hz, 1H), 7.14 (d, *J* = 8.5 Hz, 2H), 7.02 (d, *J* = 7.0 Hz, 1H), 6.85 (dd, *J* = 15.2, 8.5 Hz, 3H), 6.46 (s, 1H), 6.40 (t, *J* = 5.5 Hz, 1H), 6.03 (s, 1H), 4.84 (dd, *J* = 12.0, 5.4 Hz, 1H), 3.85 (s, 6H), 3.63 (d, *J* = 5.2 Hz, 2H), 3.56 (dd, *J* = 5.3, 2.5 Hz, 13H), 3.51 (t, *J* = 4.9 Hz, 2H), 3.47−3.33 (m, 3H), 3.22 (s, 3H), 3.19 (s, 4H), 3.12 (s, 2H), 2.83−2.60 (m, 8H). ^{13}C NMR (101 MHz, Chloroform-*d*): δ 171.63, 169.36, 169.33, 167.65, 162.89, 160.80, 155.76, 154.58, 153.31, 146.82, 136.05, 135.07, 132.51, 125.11, 117.10, 116.84, 114.01, 111.68, 110.30, 95.96, 86.90, 77.36, 77.04, 76.72, 70.71, 70.60, 70.53, 70.49, 70.27, 69.85, 69.49, 56.68, 53.17, 48.99, 48.88, 42.41, 38.79, 32.10, 31.47, 29.70, 22.86. LC−MS (ESI$^+$): calcd for $C_{49}H_{59}Cl_2N_{11}O_{12}Na$ [M + Na]$^+$, 1086.37; found, 1086.42. HPLC t_R = 31.043 min (98.40% purity).

4.1.15. 3-(2,6-Dichloro-3,5-dimethoxyphenyl)-1-(6-((4-(4-(3-((3-(2-(2,6-dioxopiperidin-3-yl)-1,3-dioxoisoindolin-5-yl)prop-2-yn-1-yl)oxy)propanoyl)piperazin-1-yl)phenyl)amino)pyrimidin-4-yl)-1-methylurea (LC-MB11). Compound LC-MB11 was synthesized in a similar manner as the bispecific compound LC-MB12, white powder (63%). ^{1}H NMR (400 MHz, chloroform-*d*): δ 12.57 (s, 1H), 9.64 (s, 1H), 8.38 (s, 1H), 7.82 (s, 1H), 7.78 (q, 2H), 7.68 (s, 1H), 7.19 (d, *J* = 8.1 Hz, 2H), 6.92 (s, 2H), 6.51 (s, 1H), 6.12 (s, 1H), 4.99 (dd, *J* = 12.1, 5.4 Hz, 1H), 4.41 (s, 2H), 3.94 (d, *J* = 6.2 Hz, 2H), 3.91 (s, 6H), 3.86−3.78 (m, 2H), 3.71 (t, *J* = 5.1 Hz, 2H), 3.29 (s, 3H), 3.19 (d, *J* = 18.1 Hz, 4H), 2.94−2.67 (m, 6H). ^{13}C NMR (101 MHz, Chloroform-*d*): δ 171.46, 169.44, 168.95, 166.71, 154.64, 153.39, 137.67, 135.07, 131.96, 130.77, 129.34, 126.72, 123.90, 113.96, 95.90, 90.23, 84.47, 77.36, 67.15, 59.24, 56.75, 49.59, 33.60, 32.22, 31.50, 22.76. LC−MS (ESI$^+$): calcd for $C_{43}H_{42}Cl_2N_9O_9$ [M + H]$^+$, 898.24; found, 898.47. HPLC t_R = 30.413 min (95.06% purity).

4.1.16. 3-(2,6-Dichloro-3,5-dimethoxyphenyl)-1-(6-((4-(4-(3-(2-(2-((2-(2,6-dioxopiperidin-3-yl)-1,3-dioxoisoindolin-5-yl)oxy)-ethoxy)ethoxy)propanoyl)piperazin-1-yl)phenyl)amino)pyrimidin-4-yl)-1-methylurea (LC-MB13). Compound LC-MB13 was synthesized in a similar manner as the bispecific compound LC-MB12, brown powder (51%). ^{1}H NMR (400 MHz, chloroform-*d*): δ 12.57 (s, 1H), 9.50 (s, 1H), 8.36 (s, 1H), 7.73 (d, *J* = 8.3 Hz, 1H), 7.69 (s, 1H), 7.28 (d, *J* = 2.2 Hz, 1H), 7.24−7.14 (m, 3H), 6.91 (s, 2H), 6.50 (s, 1H), 6.10 (s, 1H), 4.95 (dd, *J* = 12.3, 5.3 Hz, 1H), 4.18 (t, *J* = 4.6 Hz, 2H), 3.90 (s, 6H), 3.88−3.60 (m, 13H), 3.29 (s, 3H), 3.16 (s, 4H), 2.92−2.69 (m, 3H), 2.67 (t, *J* = 6.5 Hz, 2H). ^{13}C NMR (101 MHz, Chloroform-*d*): δ 171.64, 169.75, 168.96, 167.31, 167.08, 164.26, 154.63, 153.40, 135.07, 134.31, 125.60, 123.73, 121.07, 113.95, 108.92, 95.89, 77.36, 70.94, 70.52, 69.34, 68.46, 67.68, 56.74, 49.42, 33.68, 32.20, 31.69, 31.54, 22.81, 22.77, 14.25. LC−MS (ESI$^+$): calcd for $C_{44}H_{48}Cl_2N_9O_{11}$ [M + H]$^+$, 948.28; found, 948.26. HPLC t_R = 29.901 min (95.11% purity).

4.1.17. 3-(2,6-Dichloro-3,5-dimethoxyphenyl)-1-(6-((4-(4-(3-(2-(2-((2-(2,6-dioxopiperidin-3-yl)-1,3-dioxoisoindolin-5-yl)oxy)-ethoxy)ethoxy)ethoxy)propanoyl)piperazin-1-yl)phenyl)amino)-pyrimidin-4-yl)-1-methylurea (LC-MB14). Compound LC-MB14 was synthesized in a similar manner as the bispecific compound LC-MB12, brown powder (55%). ^{1}H NMR (400 MHz, chloroform-*d*): δ 12.58 (s, 1H), 9.72 (s, 1H), 8.37 (s, 1H), 7.76 (s, 1H), 7.74 (d, *J* = 8.3 Hz, 1H), 7.31 (d, *J* = 2.2 Hz, 1H), 7.24−7.15 (m, 3H), 6.93 (s, 2H), 6.50 (s, 1H), 6.11 (s, 1H), 4.95 (dd, *J* = 12.2, 5.3 Hz, 1H), 4.25−4.18 (m, 2H), 3.90 (s, 6H), 3.88−3.74 (m, 7H), 3.73−3.60 (m, 10H), 3.29 (s, 3H), 3.15 (s, 4H), 2.94−2.69 (m, 3H), 2.67 (t, *J* = 6.5 Hz, 2H). ^{13}C NMR (101 MHz, Chloroform-*d*): δ 171.70, 169.74, 169.05, 167.28, 167.12, 164.30, 154.62, 153.40, 135.06, 134.31, 125.59, 123.72, 120.96, 113.94, 109.08, 95.88, 77.36, 71.01, 70.64, 70.52, 69.43, 68.52, 67.59, 56.73, 49.40, 33.69, 32.19, 31.68, 31.55, 22.80, 22.76, 14.25. LC−MS (ESI$^+$): calcd for $C_{46}H_{51}Cl_2N_9O_{12}Na$ [M + Na]$^+$, 1014.30; found, 1014.51. HPLC t_R = 29.925 min (95.25% purity).

4.1.18. N-(2-(2-(2-(2-(4-(4-((6-(3-(2,6-Dichloro-3,5-dimethoxyphenyl)-1-methylureido)pyrimidin-4-yl)amino)phenyl)piperazin-1-yl)acetamido)ethoxy)ethoxy)ethyl)-1-(2-(2,6-dioxopiperidin-3-yl)-1,3-dioxoisoindolin-5-yl)piperidine-4-carboxamide (LC-MB15). Compound LC-MB15 was synthesized in a similar manner as the bispecific compound LC-MB1, yellow-green powder (64%). ^{1}H NMR (400 MHz, chloroform-*d*): δ 12.60 (s, 1H), 9.90 (s, 1H), 8.35 (d, *J* = 5.1 Hz, 1H), 7.75 (s, 1H), 7.62 (d, *J* = 8.5 Hz, 1H), 7.56−7.49 (m, 1H), 7.24−7.17 (m, 3H), 6.99 (dd, *J* = 8.6, 2.3 Hz, 1H), 6.91 (d, *J* = 8.6 Hz, 2H), 6.48 (d, *J* = 11.2 Hz, 2H), 6.09 (s, 1H), 4.93 (dd, *J* = 12.1, 5.3 Hz, 1H), 3.89 (s, 8H), 3.60 (s, 4H), 3.61−3.35 (m, 8H), 3.27 (s, 3H), 3.21 (t, *J* = 4.9 Hz, 4H), 3.12 (s, 2H), 2.99−2.64 (m, 11H), 1.93−1.69 (m, 4H). ^{13}C NMR (101 MHz, Chloroform-*d*): δ 174.40, 171.93, 169.56, 168.14, 167.39, 162.95, 160.74, 155.86, 155.18, 154.63, 153.47, 135.08, 134.40, 125.52, 125.02, 118.85, 117.99, 117.04, 113.93, 108.64, 95.89, 77.48, 77.36, 77.16, 76.84,

https://doi.org/10.1021/acs.jmedchem.3c00150
J. Med. Chem. XXXX, XXX, XXX−XXX

70.27, 70.24, 69.99, 69.93, 56.73, 53.40, 49.22, 47.49, 42.61, 39.20, 38.81, 32.17, 31.68, 31.60, 28.03, 22.85, 22.75, 14.24. LC−MS (ESI^+): calcd for $C_{51}H_{61}Cl_2N_{12}O_{11}$ $[M + H]^+$, 1087.39; found, 1087.62. HPLC t_R = 31.041 min (98.24% purity).

4.1.19. 3-(2,6-Dichloro-3,5-dimethoxyphenyl)-1-methyl-1-(6-((4-(4-(1-(2-(1-methyl-2,6-dioxopiperidin-3-yl)-1,3-dioxoisoindolin-5-yl)piperidine-4-carbonyl)piperazin-1-yl)phenyl)amino)pyrimidin-4-yl)urea (LC-MB12-Neg). Bispecific compound LC-MB12-Neg was synthesized in a similar manner as the bispecific compound LC-MB12, yellow-green powder (52%). ^1H NMR (400 MHz, chloroform-*d*): δ 12.60 (s, 1H), 8.35 (s, 1H), 7.68 (d, J = 8.6 Hz, 1H), 7.35 (s, 1H), 7.30−7.21 (m, 3H), 7.06 (dd, J = 8.6, 2.4 Hz, 1H), 7.01−6.93 (m, 2H), 6.51 (s, 1H), 6.11 (s, 1H), 4.98−4.89 (m, 1H), 4.03−3.93 (m, 2H), 3.91 (s, 6H), 3.84−3.77 (m, 2H), 3.76−3.69 (m, 2H), 3.30 (s, 3H), 3.27−3.15 (m, 4H), 3.20 (s, 3H), 3.11−2.92 (m, 3H), 2.86−2.68 (m, 3H), 2.05−1.81 (m, 5H). ^{13}C NMR (101 MHz, $CDCl_3$): δ 172.61, 171.36, 169.07, 168.15, 167.44, 162.83, 160.73, 155.86, 155.25, 154.56, 153.34, 148.79, 134.98, 134.37, 130.29, 125.41, 125.07, 119.28, 118.11, 117.55, 113.86, 108.76, 95.80, 87.13, 77.39, 77.07, 76.75, 56.66, 50.04, 49.90, 49.48, 47.40, 45.41, 41.67, 37.82, 32.11, 31.96, 27.89, 27.28, 22.09. LC−MS (ESI^+): calcd for $C_{44}H_{47}Cl_2N_{10}O_8$ $[M + H]^+$, 913.3; found, 913.3. HPLC t_R = 31.605 min (95.17% purity).

4.2. Molecular Modeling of the Ternary Complex of FGFR2-CRBN-PROTAC. The crystal structures of FGFR2 (PDB: 7OZY) and CRBN (PDB: 5FQD) were retrieved from the *Protein Data Bank*.[27,36] The initial binding pose of the ternary complex of FGFR2-LC-MB12-CRBN was predicted using the PROTAC-Model method.[24] All parameters of the PROTAC-Model method were set to default. The optimal predicted binding mode of the ternary complex was then subjected to conventional molecular dynamics (MD) simulations. The 200 ns MD simulation protocol was similar to that previously reported.[37] The calculation of RMSDs and extraction of representative structures of the simulated ternary complex was performed using the *CPPTRAJ* module in *Amber 20* package.[38] Molecular dynamics simulation trajectories were taken from 160 to 200 ns with 1000 snapshots utilized for per-residue decompositions based on the variable atomic dielectric-molecular mechanics/generalized Born surface area (VAD-MM/GBSA) method.[39]

4.3. Western Blot and Protein Degradation Assay. Cells were seeded in 6- or 12-well plates. PROTACs [10 mM dimethyl sulfoxide (DMSO) stock] were added to the culture medium to reach the indicated final concentrations and were incubated for the stated times. The final DMSO concentration in the culture medium was below 0.5%. The cells were then collected, washed with phosphate buffered saline (PBS), and lysed in 2× loading buffer. Protein samples were separated by sodium dodecyl sulfate polyacrylamide gel electrophoresis (SDS-PAGE), transferred to polyvinylidene difluoride (PVDF) membranes in transfer buffer, and incubated overnight at 4 °C with target antibodies diluted in 5% w/v bovine serum albumin (BSA) in phosphate buffered saline Tween (PBST). Enhanced chemiluminescence reagent (NcmECL Ultra; Cat# P10300A; NCM Biotech) was used for visualization on a Vilber Fusion FX imaging workstation. The following primary antibodies (antigen, dilution, catalogue number) were used: anti-FGFR1 (1:1000, Cat# 9740; RRID: AB_11178519), anti-FGFR2 (1:1000, Cat# 11835; RRID: AB_2797742), anti-FGFR3 (1:1000, Cat# 4574; RRID: AB_2246903), anti-FGFR4 (1:1000, Cat# 8562; RRID: AB_10891199), anti-*p*-FGFR (Tyr653/654) (1:1000, Cat# 3476; RRID: AB_331369), anti-*p*-FRS2 (Tyr196) (1:1000, Cat# 3864; RRID: AB_2106222), anti-*p*-ERK (T202/Y204) (1:2000, Cat# 4370; RRID: AB_2315112), anti-PLCγ1 antibody (1:1000, Cat# 5690), and anti-ERK (1:1000; Cat# 4695; RRID: AB_390779) was purchased from Cell Signaling Technology. Anti-CSF1R antibody (1:1000, Cat# AF0080; RRID: AB_2833269) and anti-*p*-PLCγ1(Tyr783) antibody (1:1000, Cat# AF3210) were purchased from Affinity Biosciences. Anti-β-actin (1:5000, Cat. no. R1207-1) antibodies and HRP-conjugated goat anti-rabbit IgG secondary antibodies (1:100,000, Cat# HA1001) were purchased from Huabio. Grayscale analysis was performed using ImageJ software.

4.4. Kinase Selectivity Profiling. The kinase selectivity profile of LC-MB12 was tested using the Eurofins KINOMEscan platform (https://www.eurofinsdiscoveryservices.com/). LC-MB12 was screened at 1 μM against a scanEDGE panel with 97 kinase targets. The results of the screening are presented as '% Ctrl, with lower numbers indicating stronger inhibition.

4.5. Proliferation Assay of Ba/F3-TEL-FGFR Cell Lines. Ba/F3 stable cells (RRID: CVCL_0161) were suspended in 96-well plates. Five microliters of 20× LC-MB12 was added to a 96-well plate. The final DMSO concentration in each well was 0.1%. After incubation for 72 h, 50 μL of CellTiter-Glo reagent (Promega, Cat# G7573) was added to each well and incubated at room temperature for 10 min to stabilize the luminescent signal. Luminescence was recorded using a SpectraMax Paradigm microplate reader (Molecular Devices). Inhibition rate (Inh %) = 100 − (RLU compound − RLU blank)/(RLU control − RLU blank) × 100%. Data were analyzed using GraphPad Prism 7.0 fitted to a 4-parameter equation to generate concentration response curves.

4.6. Flow Cytometry. The surface FGFR2 level in KATO III cells (RRID: CVCL_0371) was assessed by flow cytometry. Approximately 2×10^6 cells were seeded in 6-well plates and treated with DMSO, BGJ398, or LC-MB12 for 6 h. The cells were washed with cold PBS and incubated with anti-FGFR2 antibody (1:100, Cat# 23328; RRID: AB_2798862, Cell Signaling Technology) at 4 °C for 1 h. The cells were washed three times with 1 mL ″ice-cold PBS and incubated with Alexa Fluor 488-conjugated secondary antibody (1:500, Cat# A0423, Beyotime Biotechnology) at 4 °C for 1 h. Finally, the cells were washed with cold PBS and re-suspended in 1 mL of cold PBS. Fluorescence-assisted cell sorting analysis was performed using an BD Accuri C6 Plus flow cytometer (BD Biosciences) and analyzed using FlowJo software (BD Biosciences). A minimum of 100,000 events were measured following excitation with an argon laser at 488 nm and emission using an FITC detector (519 nm).

The cell cycle was analyzed using a cell cycle staining kit (Cat# CCS012, Multisciences). Briefly, KATO III cells were harvested with trypsin without ethylenediaminetetraacetic acid (EDTA) (Cat# BC-CE-006, Bio-channel), followed by two washes with 1 mL cold PBS. Cells were pelleted by centrifugation and fixed by resuspension in cold 70% ethanol overnight at −20 °C. The cells were washed with 1 mL of cold PBS, resuspended in 1 mL of DNA staining solution, incubated at room temperature for 30 min, followed by flow cytometry analysis.

4.7. Immunofluorescence. KATO III cells treated with 100 nM BGJ398 or LC-MB12 were fixed with 2% formaldehyde in PBS for 2 min and blocked with 5% w/v BSA in PBS for 1 h. Cells were incubated with anti-FGFR2 antibody (Cat# R1310-10, Huabio) overnight. Cells were washed with PBS three times, incubated with Alexa Fluor 488-conjugated secondary antibody (Cat# A0423; Beyotime Biotechnology) for 1 h, and stained with DAPI (4′,6-diamidino-2-phenylindole, Cat# C1002, Beyotime Biotechnology) for 10 min. Cells were then observed by fluorescence microscopy using an EVOS M7000 imaging system (Thermo Fisher Scientific).

4.8. Plasma Protein Binding. The binding of LC-MB12 to plasma proteins was evaluated in dog, rat, and mouse plasma using the equilibrium dialysis method. Briefly, 0.5 mmol/L of the compound was incubated in plasma at 37 °C for 5 h. After incubation, aliquots both from the donor and receiver sides of the dialysis apparatus were used for new sample preparation plates and mixed with the opposite matrixes. The concentrations in the supernatant were determined by using quantitative LC−MS/MS (TQ-6500+). Calibration and quality control samples were prepared using blank plasma and internal standards as follows: % Bound = 100 × ($[Donor]_{5h}$ − $[Receiver]_{5h}$)/$[Donor]_{5h}$. Fu (%) = 100 − % Bound.

4.9. Animal Study. The PK parameters of LC-MB12 were tested by Shanghai Medicilon Inc (Medicilon.com). LC-MB12 was dissolved in a vehicle containing 10% Solutol, 85% (10% HP--CD in saline), and 5% DMSO. The pH was adjusted to 9−10. Male Sprague Dawley (SD) rats were administered LC-MB12 solution intravenously (i.v.) at 3 mg/kg and p.o. at 20 mg/kg. Blood samples from each experimental

https://doi.org/10.1021/acs.jmedchem.3c00150
J. Med. Chem. XXXX, XXX, XXX−XXX

rat were collected at 0.25, 0.5, 1, 2, 4, 6, 8, and 24 h (p.o.) or 0.083, 0.25, 0.5, 1, 2, 4, 8, and 24 h (i.v.) post-treatment, and centrifuged.

Plasma supernatant samples were analyzed using LC−MS/MS (TQ6500+).

For preliminary toxicity evaluation, oral doses of 20 mg/kg/day LC-MB12 were tested in ICR mice. Mortality and clinical symptoms of toxicity were monitored daily for 30 days. After that, the rats were subjected to biochemical investigation, weight measurement of the body and organs, and hematological assay.

The tumor xenograft experiment involved randomly dividing 5 week old female BALB/c nude mice (20−22 g) into three groups based on body weight. A suspension of 5×10^6/mL SNU-16 cells (RRID: CVCL_0076) was subcutaneously injected into the right flank of nude mice. The average tumor volume in the mice reached 50−100 mm^3. BGJ398 and LC-MB12 were formulated in 0.5% CMC-Na by intragastric administration (20 mg/kg/day). Control mice were orally administered with equal volumes of 0.5% CMC-Na vehicle. The body weights and tumor volumes of the mice were measured every 2 days. The tumor volume was confirmed by measuring the width (w) and length (l) at the indicated time points. Tumor samples were harvested at the last dose after 4 h of treatment and used for further studies. This study was approved by the Institutional Animal Care and Use Committee of Hangzhou Medical College, China (2022-005).

4.10. Statistical Analysis. The significance analysis was conducted by unpaired, ordinary one-way ANOVA with Dunnett's multiple comparison using GraphPad Prism 8.0. Differences between the groups were considered statistically significant at $P < 0.05$.

■ ASSOCIATED CONTENT

Supporting Information

The Supporting Information is available free of charge at https://pubs.acs.org/doi/10.1021/acs.jmedchem.3c00150.

Additional cell-based experiments and NMR, MS, and HPLC spectral information (PDF)

Molecular formula strings (CSV)

■ AUTHOR INFORMATION

Corresponding Authors

Lingfeng Chen − *Affiliated Yongkang First People's Hospital and School of Pharmacy, Hangzhou Medical College, Hangzhou 310012 Zhejiang, China*; orcid.org/0000-0003-0089-6559; Phone: +86-571-88215622; Email: lfchen@hmc.edu.cn

Guang Liang − *Affiliated Yongkang First People's Hospital and School of Pharmacy, Hangzhou Medical College, Hangzhou 310012 Zhejiang, China*; Email: wzmcliangguang@163.com

Lulu Zheng − *Department of Pharmacy, Tongde Hospital of Zhejiang Province, Hangzhou, Zhejiang 310000, China*; Email: unasetty@163.com

Authors

Lin Ma − *Affiliated Yongkang First People's Hospital and School of Pharmacy, Hangzhou Medical College, Hangzhou 310012 Zhejiang, China*

Yingying Li − *Affiliated Yongkang First People's Hospital and School of Pharmacy, Hangzhou Medical College, Hangzhou 310012 Zhejiang, China*

Ruixiang Luo − *Affiliated Yongkang First People's Hospital and School of Pharmacy, Hangzhou Medical College, Hangzhou 310012 Zhejiang, China*

Yuhan Wang − *Affiliated Yongkang First People's Hospital and School of Pharmacy, Hangzhou Medical College, Hangzhou 310012 Zhejiang, China*

Jiaqi Cao − *Affiliated Yongkang First People's Hospital and School of Pharmacy, Hangzhou Medical College, Hangzhou 310012 Zhejiang, China*

Weitao Fu − *Department of Computer-Aided Drug Design, Jiangsu Vcare PharmaTech Co. Ltd., Nanjing 211800, China*

Bolan Qian − *Affiliated Yongkang First People's Hospital and School of Pharmacy, Hangzhou Medical College, Hangzhou 310012 Zhejiang, China*

Lei Zheng − *Affiliated Yongkang First People's Hospital and School of Pharmacy, Hangzhou Medical College, Hangzhou 310012 Zhejiang, China*

Longguang Tang − *International Institutes of Medicine, The Fourth Affiliated Hospital, Zhejiang University School of Medicine, Zhejiang 322000, China*

Xinting Lv − *Affiliated Yongkang First People's Hospital and School of Pharmacy, Hangzhou Medical College, Hangzhou 310012 Zhejiang, China*

Complete contact information is available at: https://pubs.acs.org/10.1021/acs.jmedchem.3c00150

Author Contributions

$^{\perp}$L.M., Y.L., and R.L. contributed equally to this work.

Author Contributions

L.C., G.L., and L.M. conceived and proposed this project. L.M. and Y.W. synthesized the target compounds. Y.L., R.L., J.C., and B.Q. completed drug screening and cell-based studies. L.M. and W.F. completed the molecular docking study. L.M. and L.Z. participated in the in vivo antitumor study. L.T., L.Z., and X.L. contributed to the reviewing of the manuscript. R.L. conducted flow cytometry assays. L.C. wrote the manuscript with input from all authors.

Notes

The authors declare no competing financial interest.

■ ACKNOWLEDGMENTS

This work was supported by the National Natural Science Foundation of China (82103999 to L.C.), the Natural Science Funding of Zhejiang Province (LQ22H300007 to L.C.), the Zhejiang Health Program (YS2022004 to L.C.), the Zhejiang Medical and Health Science Project (2023KY622 to L.Z.), and the Zhejiang Provincial Key Scientific Project (2021C03041 to G.L.).

■ ABBREVIATIONS

DMSO, dimethyl sulfoxide; FGF, fibroblast growth factor; FGFRs, fibroblast growth factor receptors; Fu %, fraction unbound %; MD, molecular dynamics; PEG, polyethylene glycol; POI, protein of interest; PROTAC, proteolysis-targeting chimeras; RMSDs, root-mean-square deviations; RTKs, receptor tyrosine kinases; UPS, ubiquitin/proteasome system; VHL, von Hippel−Lindau

■ REFERENCES

(1) Beenken, A.; Mohammadi, M. The FGF family: biology, pathophysiology and therapy. *Nat. Rev. Drug Discov.* **2009**, *8*, 235−253.

(2) Katoh, M.; Nakagama, H. FGF receptors: cancer biology and therapeutics. *Med. Res. Rev.* **2014**, *34*, 280−300.

(3) Chen, L.; Marsiglia, W. M.; Chen, H.; Katigbak, J.; Erdjument-Bromage, H.; Kemble, D. J.; Fu, L.; Ma, J.; Sun, G.; Zhang, Y.; et al. Molecular basis for receptor tyrosine kinase A-loop tyrosine transphosphorylation. *Nat. Chem. Biol.* **2020**, *16*, 267−277.

(4) Eswarakumar, V. P.; Lax, I.; Schlessinger, J. Cellular signaling by fibroblast growth factor receptors. *Cytokine Growth Factor Rev.* **2005**, *16*, 139−149.
(5) (a) Babina, I. S.; Turner, N. C. Advances and challenges in targeting FGFR signalling in cancer. *Nat. Rev. Cancer* **2017**, *17*, 318−332. (b) Katoh, M. Therapeutics Targeting FGF Signaling Network in Human Diseases. *Trends Pharmacol. Sci.* **2016**, *37*, 1081−1096.
(6) Chen, L.; Zhang, Y.; Yin, L.; Cai, B.; Huang, P.; Li, X.; Liang, G. Fibroblast growth factor receptor fusions in cancer: opportunities and challenges. *J. Exp. Clin. Cancer Res.* **2021**, *40*, 345.
(7) Jogo, T.; Nakamura, Y.; Shitara, K.; Bando, H.; Yasui, H.; Esaki, T.; Terazawa, T.; Satoh, T.; Shinozaki, E.; Nishina, T.; et al. Circulating Tumor DNA Analysis Detects FGFR2 Amplification and Concurrent Genomic Alterations Associated with FGFR Inhibitor Efficacy in Advanced Gastric Cancer. *Clin. Cancer Res.* **2021**, *27*, 5619−5627.
(8) Sia, D.; Losic, B.; Moeini, A.; Cabellos, L.; Hao, K.; Revill, K.; Bonal, D.; Miltiadous, O.; Zhang, Z.; Hoshida, Y.; et al. Massive parallel sequencing uncovers actionable FGFR2-PPHLN1 fusion and ARAF mutations in intrahepatic cholangiocarcinoma. *Nat. Commun.* **2015**, *6*, 6087.
(9) (a) Eathiraj, S.; Palma, R.; Hirschi, M.; Volckova, E.; Nakuci, E.; Castro, J.; Chen, C. R.; Chan, T. C.; France, D. S.; Ashwell, M. A. A novel mode of protein kinase inhibition exploiting hydrophobic motifs of autoinhibited kinases: discovery of ATP-independent inhibitors of fibroblast growth factor receptor. *J. Biol. Chem.* **2011**, *286*, 20677−20687. (b) Hall, T. G.; Yu, Y.; Eathiraj, S.; Wang, Y.; Savage, R. E.; Lapierre, J. M.; Schwartz, B.; Abbadessa, G. Preclinical Activity of ARQ 087, a Novel Inhibitor Targeting FGFR Dysregulation. *PLoS One* **2016**, *11*, No. e0162594. (c) Mazzaferro, V.; El-Rayes, B. F.; Droz Dit Busset, M.; Cotsoglou, C.; Harris, W. P.; Damjanov, N.; Masi, G.; Rimassa, L.; Personeni, N.; Braiteh, F.; et al. Derazantinib (ARQ 087) in advanced or inoperable FGFR2 gene fusion-positive intrahepatic cholangiocarcinoma. *Br. J. Cancer* **2019**, *120*, 165−171. (d) Papadopoulos, K. P.; El-Rayes, B. F.; Tolcher, A. W.; Patnaik, A.; Rasco, D. W.; Harvey, R. D.; LoRusso, P. M.; Sachdev, J. C.; Abbadessa, G.; Savage, R. E.; et al. A Phase 1 study of ARQ 087, an oral pan-FGFR inhibitor in patients with advanced solid tumours. *Br. J. Cancer* **2017**, *117*, 1592−1599.
(10) (a) Loriot, Y.; Necchi, A.; Park, S. H.; Garcia-Donas, J.; Huddart, R.; Burgess, E.; Fleming, M.; Rezazadeh, A.; Mellado, B.; Varlamov, S.; et al. Erdafitinib in Locally Advanced or Metastatic Urothelial Carcinoma. *N. Engl. J. Med.* **2019**, *381*, 338−348. (b) Patani, H.; Bunney, T. D.; Thiyagarajan, N.; Norman, R. A.; Ogg, D.; Breed, J.; Ashford, P.; Potterton, A.; Edwards, M.; Williams, S. V.; et al. Landscape of activating cancer mutations in FGFR kinases and their differential responses to inhibitors in clinical use. *Oncotarget* **2016**, *7*, 24252−24268. (c) Abou-Alfa, G. K.; Sahai, V.; Hollebecque, A.; Vaccaro, G.; Melisi, D.; Al-Rajabi, R.; Paulson, A. S.; Borad, M. J.; Gallinson, D.; Murphy, A. G.; et al. Pemigatinib for previously treated, locally advanced or metastatic cholangiocarcinoma: a multicentre, open-label, phase 2 study. *Lancet Oncol.* **2020**, *21*, 671−684. (d) Romero, D. Benefit from pemigatinib in cholangiocarcinoma. *Nat. Rev. Clin. Oncol.* **2020**, *17*, 337.
(11) Javle, M.; Lowery, M.; Shroff, R. T.; Weiss, K. H.; Springfeld, C.; Borad, M. J.; Ramanathan, R. K.; Goyal, L.; Sadeghi, S.; Macarulla, T.; et al. Phase II Study of BGJ398 in Patients With FGFR-Altered Advanced Cholangiocarcinoma. *J. Clin. Oncol.* **2018**, *36*, 276−282.
(12) Goyal, L.; Shi, L.; Liu, L. Y.; Fece de la Cruz, F.; Lennerz, J. K.; Raghavan, S.; Leschiner, I.; Elagina, L.; Siravegna, G.; Ng, R. W. S.; et al. TAS-120 Overcomes Resistance to ATP-Competitive FGFR Inhibitors in Patients with FGFR2 Fusion-Positive Intrahepatic Cholangiocarcinoma. *Cancer Discov.* **2019**, *9*, 1064−1079.
(13) (a) Goyal, L.; Saha, S. K.; Liu, L. Y.; Siravegna, G.; Leshchiner, I.; Ahronian, L. G.; Lennerz, J. K.; Vu, P.; Deshpande, V.; Kambadakone, A.; et al. Polyclonal Secondary FGFR2 Mutations Drive Acquired Resistance to FGFR Inhibition in Patients with FGFR2 Fusion-Positive Cholangiocarcinoma. *Cancer Discov.* **2017**, *7*, 252−263. (b) Saborowski, A.; Lehmann, U.; Vogel, A. FGFR inhibitors in cholangiocarcinoma: what's now and what's next? *Ther. Adv. Med. Oncol.* **2020**, *12*, 175883592095329.
(14) (a) Chen, L.; Fu, W.; Zheng, L.; Liu, Z.; Liang, G. Recent Progress of Small-Molecule Epidermal Growth Factor Receptor (EGFR) Inhibitors against C797S Resistance in Non-Small-Cell Lung Cancer. *J. Med. Chem.* **2018**, *61*, 4290−4300. (b) Woyach, J. A.; Furman, R. R.; Liu, T. M.; Ozer, H. G.; Zapatka, M.; Ruppert, A. S.; Xue, L.; Li, D. H.; Steggerda, S. M.; Versele, M.; et al. Resistance mechanisms for the Bruton's tyrosine kinase inhibitor ibrutinib. *N. Engl. J. Med.* **2014**, *370*, 2286−2294.
(15) (a) Chen, G.; Liu, Y.; Goetz, R.; Fu, L.; Jayaraman, S.; Hu, M. C.; Moe, O. W.; Liang, G.; Li, X.; Mohammadi, M. α-Klotho is a non-enzymatic molecular scaffold for FGF23 hormone signalling. *Nature* **2018**, *553*, 461−466. (b) Lee, S.; Choi, J.; Mohanty, J.; Sousa, L. P.; Tome, F.; Pardon, E.; Steyaert, J.; Lemmon, M. A.; Lax, I.; Schlessinger, J. Structures of beta-klotho reveal a 'zip code'-like mechanism for endocrine FGF signalling. *Nature* **2018**, *553*, 501−505.
(16) Meric-Bernstam, F.; Bahleda, R.; Hierro, C.; Sanson, M.; Bridgewater, J.; Arkenau, H. T.; Tran, B.; Kelley, R. K.; Park, J. O.; Javle, M.; et al. Futibatinib, an Irreversible FGFR1-4 Inhibitor, in Patients with Advanced Solid Tumors Harboring FGF/FGFR Aberrations: A Phase I Dose-Expansion Study. *Cancer Discov.* **2022**, *12*, 402−415.
(17) Burslem, G. M.; Crews, C. M. Proteolysis-Targeting Chimeras as Therapeutics and Tools for Biological Discovery. *Cell* **2020**, *181*, 102−114.
(18) Du, G.; Jiang, J.; Wu, Q.; Henning, N. J.; Donovan, K. A.; Yue, H.; Che, J.; Lu, W.; Fischer, E. S.; Bardeesy, N.; et al. Discovery of a Potent Degrader for Fibroblast Growth Factor Receptor 1/2. *Angew Chem. Int. Ed. Engl.* **2021**, *60*, 15905−15911.
(19) (a) Huang, H. T.; Dobrovolsky, D.; Paulk, J.; Yang, G.; Weisberg, E. L.; Doctor, Z. M.; Buckley, D. L.; Cho, J. H.; Ko, E.; Jang, J.; et al. A Chemoproteomic Approach to Query the Degradable Kinome Using a Multi-kinase Degrader. *Cell Chem. Biol.* **2018**, *25*, 88−99.e6. (b) Jiang, B.; Wang, E. S.; Donovan, K. A.; Liang, Y.; Fischer, E. S.; Zhang, T.; Gray, N. S. Development of Dual and Selective Degraders of Cyclin-Dependent Kinases 4 and 6. *Angew Chem. Int. Ed. Engl.* **2019**, *58*, 6321−6326. (c) Olson, C. M.; Jiang, B.; Erb, M. A.; Liang, Y.; Doctor, Z. M.; Zhang, Z.; Zhang, T.; Kwiatkowski, N.; Boukhali, M.; Green, J. L.; et al. Pharmacological perturbation of CDK9 using selective CDK9 inhibition or degradation. *Nat. Chem. Biol.* **2018**, *14*, 163−170.
(20) Burslem, G. M.; Smith, B. E.; Lai, A. C.; Jaime-Figueroa, S.; McQuaid, D. C.; Bondeson, D. P.; Toure, M.; Dong, H.; Qian, Y.; Wang, J.; et al. The Advantages of Targeted Protein Degradation Over Inhibition: An RTK Case Study. *Cell Chem. Biol.* **2018**, *25*, 67−77.e3.
(21) Pike, A.; Williamson, B.; Harlfinger, S.; Martin, S.; McGinnity, D. F. Optimising proteolysis-targeting chimeras (PROTACs) for oral drug delivery: a drug metabolism and pharmacokinetics perspective. *Drug Discovery Today* **2020**, *25*, 1793−1800.
(22) Fischer, E. S.; Bohm, K.; Lydeard, J. R.; Yang, H.; Stadler, M. B.; Cavadini, S.; Nagel, J.; Serluca, F.; Acker, V.; Lingaraju, G. M.; et al. Structure of the DDB1-CRBN E3 ubiquitin ligase in complex with thalidomide. *Nature* **2014**, *512*, 49−53.
(23) Wang, M.; Lu, J.; Wang, M.; Yang, C. Y.; Wang, S. Discovery of SHP2-D26 as a First, Potent, and Effective PROTAC Degrader of SHP2 Protein. *J. Med. Chem.* **2020**, *63*, 7510−7528.
(24) Weng, G.; Li, D.; Kang, Y.; Hou, T. Integrative Modeling of PROTAC-Mediated Ternary Complexes. *J. Med. Chem.* **2021**, *64*, 16271−16281.
(25) Cao, C.; He, M.; Wang, L.; He, Y.; Rao, Y. Chemistries of bifunctional PROTAC degraders. *Chem. Soc. Rev.* **2022**, *51*, 7066−7114.
(26) (a) Sase, H.; Nakanishi, Y.; Aida, S.; Horiguchi-Takei, K.; Akiyama, N.; Fujii, T.; Sakata, K.; Mio, T.; Aoki, M.; Ishii, N. Acquired JHDM1D-BRAF Fusion Confers Resistance to FGFR Inhibition in FGFR2-Amplified Gastric Cancer. *Mol. Cancer Ther.* **2018**, *17*, 2217−2225. (b) Kunii, K.; Davis, L.; Gorenstein, J.; Hatch,

https://doi.org/10.1021/acs.jmedchem.3c00150
J. Med. Chem. XXXX, XXX, XXX−XXX

H.; Yashiro, M.; Di Bacco, A.; Elbi, C.; Lutterbach, B. FGFR2-amplified gastric cancer cell lines require FGFR2 and Erbb3 signaling for growth and survival. *Cancer Res.* **2008**, *68*, 2340−2348.
(27) Turner, L. D.; Trinh, C. H.; Hubball, R. A.; Orritt, K. M.; Lin, C. C.; Burns, J. E.; Knowles, M. A.; Fishwick, C. W. G. From Fragment to Lead: De Novo Design and Development toward a Selective FGFR2 Inhibitor. *J. Med. Chem.* **2022**, *65*, 1481−1504.
(28) Shvartsbart, A.; Roach, J. J.; Witten, M. R.; Koblish, H.; Harris, J. J.; Covington, M.; Hess, R.; Lin, L.; Frascella, M.; Truong, L.; et al. Discovery of Potent and Selective Inhibitors of Wild-Type and Gatekeeper Mutant Fibroblast Growth Factor Receptor (FGFR) 2/3. *J. Med. Chem.* **2022**, *65*, 15433−15442.
(29) Law, R. P.; Nunes, J.; Chung, C. W.; Bantscheff, M.; Buda, K.; Dai, H.; Evans, J. P.; Flinders, A.; Klimaszewska, D.; Lewis, A. J.; et al. Discovery and Characterisation of Highly Cooperative FAK-Degrading PROTACs. *Angew Chem. Int. Ed. Engl.* **2021**, *60*, 23327−23334.
(30) Cantley, J.; Ye, X.; Rousseau, E.; Januario, T.; Hamman, B. D.; Rose, C. M.; Cheung, T. K.; Hinkle, T.; Soto, L.; Quinn, C.; et al. Selective PROTAC-mediated degradation of SMARCA2 is efficacious in SMARCA4 mutant cancers. *Nat. Commun.* **2022**, *13*, 6814.
(31) Wang, L.; Shao, X.; Zhong, T.; Wu, Y.; Xu, A.; Sun, X.; Gao, H.; Liu, Y.; Lan, T.; Tong, Y.; et al. Discovery of a first-in-class CDK2 selective degrader for AML differentiation therapy. *Nat. Chem. Biol.* **2021**, *17*, 567−575.
(32) Chen, L.; Chen, Y.; Zhang, C.; Jiao, B.; Liang, S.; Tan, Q.; Chai, H.; Yu, W.; Qian, Y.; Yang, H.; et al. Discovery of First-In-Class Potent and Selective Tropomyosin Receptor Kinase Degraders. *J. Med. Chem.* **2020**, *63*, 14562−14575.
(33) Bondeson, D. P.; Smith, B. E.; Burslem, G. M.; Buhimschi, A. D.; Hines, J.; Jaime-Figueroa, S.; Wang, J.; Hamman, B. D.; Ishchenko, A.; Crews, C. M. Lessons in PROTAC Design from Selective Degradation with a Promiscuous Warhead. *Cell Chem. Biol.* **2018**, *25*, 78−87.e5.
(34) Gadd, M. S.; Testa, A.; Lucas, X.; Chan, K. H.; Chen, W.; Lamont, D. J.; Zengerle, M.; Ciulli, A. Structural basis of PROTAC cooperative recognition for selective protein degradation. *Nat. Chem. Biol.* **2017**, *13*, 514−521.
(35) Ruffilli, C.; Roth, S.; Rodrigo, M.; Boyd, H.; Zelcer, N.; Moreau, K. Proteolysis Targeting Chimeras (PROTACs): A Perspective on Integral Membrane Protein Degradation. *ACS Pharmacol. Transl. Sci.* **2022**, *5*, 849−858.
(36) Petzold, G.; Fischer, E. S.; Thoma, N. H. Structural basis of lenalidomide-induced CK1α degradation by the CRL4CRBN ubiquitin ligase. *Nature* **2016**, *532*, 127−130.
(37) (a) Fu, W.; Zhang, M.; Liao, J.; Tang, Q.; Lei, Y.; Gong, Z.; Shan, L.; Duan, M.; Chai, X.; Pang, J.; et al. Discovery of a Novel Androgen Receptor Antagonist Manifesting Evidence to Disrupt the Dimerization of the Ligand-Binding Domain via Attenuating the Hydrogen-Bonding Network Between the Two Monomers. *J. Med. Chem.* **2021**, *64*, 17221−17238. (b) Fu, W.; Wang, E.; Ke, D.; Yang, H.; Chen, L.; Shao, J.; Hu, X.; Xu, L.; Liu, N.; Hou, T. Discovery of a Novel Fusarium Graminearum Mitogen-Activated Protein Kinase (FgGpmk1) Inhibitor for the Treatment of Fusarium Head Blight. *J. Med. Chem.* **2021**, *64*, 13841−13852.
(38) Roe, D. R.; Cheatham, T. E., III PTRAJ and CPPTRAJ: software for processing and analysis of molecular dynamics trajectory data. *J. Chem. Theory Comput.* **2013**, *9*, 3084−3095.
(39) Wang, E.; Fu, W.; Jiang, D.; Sun, H.; Wang, J.; Zhang, X.; Weng, G.; Liu, H.; Tao, P.; Hou, T. VAD-MM/GBSA: A Variable Atomic Dielectric MM/GBSA Model for Improved Accuracy in Protein-Ligand Binding Free Energy Calculations. *J. Chem. Inf. Model.* **2021**, *61*, 2844−2856.

https://doi.org/10.1021/acs.jmedchem.3c00150
J. Med. Chem. XXXX, XXX, XXX−XXX